**SCHOOL OF ADVANCED STUDIES OF THE ROMANIAN ACADEMY**
**DOCTORAL SCHOOL OF CHEMICAL SCIENCES "PETRU PONI"**
**INSTITUTE OF MACROMOLECULAR CHEMISTRY**
**CHEMISTRY Field**

***POLYMER–CYCLODEXTRIN CONJUGATES: SYNTHESIS, PROPERTIES, AND APPLICATIONS***

# PHD THESIS SUMMARY

**SCIENTIFIC COORDINATOR:**
DR. VALERIA HARABAGIU

**PhD STUDENT:**
ALEXANDRA-DIANA DIACONU
(married DABIJA)

2026

**Contents**

# INTRODUCTION

Polyurethanes (PU) represent a versatile class of polymeric materials in terms of their mechanical and physical properties. These properties can be tailored through careful manipulation of their chemical structure and synthesis conditions. Typically, PU are obtained via polyaddition reactions between a diisocyanate and a compound containing hydroxyl (OH) groups, such as diols and polyols [1].

In recent years, polyurethane materials derived from renewable components, such as cyclodextrins, have attracted considerable attention due to their remarkable characteristics from a green chemistry perspective [2–4]. Cyclodextrins (CD), cyclic oligosaccharides enzymatically derived from starch, are composed of glucose units and feature a hydrophobic cavity that allows them to form inclusion complexes with a variety of hydrophobic molecules [5]. This property makes them particularly valuable in pharmaceutical applications [6–9], wastewater treatment [10], and the food industry [11]. However, the low solubility of CD represents a significant limitation in the synthesis or processing of CD-conjugated materials. To overcome this limitation, various chemical modification strategies are employed. One interesting approach is the derivatization of CD via esterification of the OH groups with polyester chains, which additionally confer biodegradability [12]. The preparation of CD modified with oligoesters results in significant changes to the material properties. An important feature of these products, besides retaining the ability to encapsulate small molecules within the CD cavity, is the increased solubility in dimethylformamide (DMF) compared to native CD. Moreover, introducing sequences susceptible to hydrolytic degradation presents an advantage in biomedical applications.

CD-containing polyurethane materials can be obtained either directly or stepwise, through the incorporation of additional polymer chains. The latter approach involves a two-step synthesis: the first step consists of forming a prepolymer with terminal isocyanate (NCO) groups, while in the second step, the OH groups of the CD react with the NCO groups of the prepolymer. The prepolymerization stage plays a key role in the preparation of polyurethanes and can influence the properties of the final materials [13]. Depending on the nature of the isocyanate groups and the functionality of the polyols, the resulting reaction mixture is complex, potentially containing unreacted polyol, polyol with a single OH group reacted, polyol with multiple OH groups reacted, and elongated polymer chains containing two or more oligodiols in a single chain [14]. Regardless

of the synthesis strategy, whether direct or stepwise, the combination of these elements leads to materials that integrate the excellent properties of both PU and CD.

Characterization of the reaction mixture during prepolymerization is essential for optimizing the synthesis process. Matrix-assisted laser desorption/ionization mass spectrometry (MALDI-MS) is a particularly useful analytical technique for polymer analysis, providing detailed information on molecular weight [15] and the composition of the polyol–diisocyanate system at different stages of the reaction [14]. The data provided by this method allows for a deep understanding of reaction kinetics, facilitating precise adjustment of polymerization conditions to obtain materials with specific properties.

The growing interest in using CD molecules in combination with biodegradable polymers is related to the formation of host–guest physical interactions that result in supramolecular systems capable of encapsulating hydrophobic substances [16,17]. Furthermore, the incorporation of CD modified with biodegradable polymers into the polyurethane network also enables the production of networks susceptible to hydrolytic cleavage. This is of particular interest, as most conventional polyurethane systems are not biodegradable.

In this context, the present thesis aims to make an original contribution to the existing scientific literature by preparing biodegradable polyurethane systems through the inclusion of hydrolyzable linkages within the internal structure. The materials are produced via polyaddition reactions between diisocyanates and esterified CD, in the form of gels or submicron particles. The novelty of this work lies in the use of new CD derivatives with controlled structural design to influence the course of crosslinking reactions. Initially, a thorough understanding of phenomena affecting prepolymer synthesis was sought through advanced structural characterization, particularly MALDI-MS. Original methods were developed to monitor the synthesis processes. Additionally, the influence of the structure of the starting compounds on the crosslinking reactions was correlated with the physical properties of the obtained materials to demonstrate their potential applications. Special attention was given to understanding the biodegradability of the synthesized materials. Thus, the CD-containing biodegradable polyurethane materials were investigated in absorption and release processes of different molecules for biomedical or environmental protection applications.

The work aimed to achieve three specific objectives, namely: **O1** – Establishing methods for the preparation of polymer–cyclodextrin conjugate-based networks with controlled structures; **O2** –

Processing the networks in the form of gels and micro/nanoparticles; **O3** – Investigating the influence of the nature and properties of the polymeric materials on their potential applications, including the networks' capacity for complexation/release of various organic compounds with biological activity, and wastewater purification through physical complexation of pollutants.

The thesis is structured into two parts. **Part I** (**Chapter 1**) presents the literature data that guided the study, while **Part II** (**Chapters 2–5**) contains the experimental methods and the main results obtained during the research.

In **Chapter 1**, general aspects of CD and PU are briefly presented, along with methods for incorporating cyclodextrins into polyurethane networks, the influence of cyclodextrins in these networks, and the characterization techniques of prepolymers used in multicomponent polyaddition reactions.

**Chapter 2** focused on optimizing the synthesis of prepolymers with terminal isocyanate groups and their structural characterization using MALDI mass spectrometry. The first study investigated how different reaction parameters (temperature, solvent amount, and catalyst quantity) influence the polyaddition process of polyethylene glycol (PEG) to isophorone diisocyanate (IPDI), which leads to the formation of the prepolymer. The second study aimed to prepare a prepolymer using the reaction between β-CD and IPDI, a system with a higher complexity due to the large number of OH groups present in the β-CD molecule.

**Chapter 3** describes the preparation, structural characterization, and properties of a series of nanoporous particles based on cyclodextrin modified with oligolactide (CDLA). These materials were obtained through the direct reaction of three types of oligolactide-modified cyclodextrins (α-, β-, and γ-CDLA) with IPDI. The influence of solvent quantity and CD type on the outcome of the synthesis reaction was studied. The resulting polyaddition products were subjected to mechanical milling to produce nanoscale particles, and their adsorption capacity for a cationic and an anionic dye was determined.

**Chapter 4** presents a comparative study of three polyurethane networks containing β-CD, β-CDLA, and β-CD modified with oligocaprolactone (β-CDCL). Initially, differences in the polyaddition reaction of native β-CD and its substituted derivatives (β-CDLA and β-CDCL) with the PEG–diisocyanate prepolymer (PEG-$(NCO)_2$) were investigated. Subsequently, the influence of chemical structure on the properties of the resulting materials was examined. The degradable

nature of all networks and the potential for controlled drug release from networks containing short oligoester chains attached to the CD molecule were also studied.

The materials and characterization methods used to perform the experiments are described in **Chapter 5**.

The thesis concludes with the general conclusions, a section on the dissemination of results obtained during the doctoral stage, and the reference list.

# PART II. PERSONAL CONTRIBUTIONS

# CHAPTER 2. STRUCTURAL CHARACTERIZATION BY MALDI-MS OF PREPOLYMERS WITH ISOCYANATE FUNCTIONALITIES

## 2.2. Investigation of the formation reaction of polyethylene glycol–isophorone diisocyanate prepolymers

The polyaddition reaction between PEG and IPDI is illustrated in **Scheme 2.1**. As shown, the formation of the target compound, difunctionalized PEG (P2' in **Scheme 2.1**), involves an initial polyaddition step between PEG (P0) and IPDI, leading to the formation of mono-functionalized species denoted as P1'. The unreacted OH groups of the P1' chains subsequently react with IPDI, resulting in the difunctionalized product, labeled P2'. Meanwhile, the reactive NCO groups of the P1' or P2' products may react with other OH groups in the reaction mixture (from P0 or P1'), leading to undesired secondary products, such as the linkage of two or more oligomeric sequences. Thus, the effect of reaction parameters—including reaction temperature, reactant concentration in DMF, and catalyst amount (**Table 2.1**)—was investigated, while the molar ratio of PEG to IPDI was kept constant at 1:2. Fractions of the reaction mixture were collected at specific time intervals and subsequently analyzed by MALDI-MS under defined conditions.

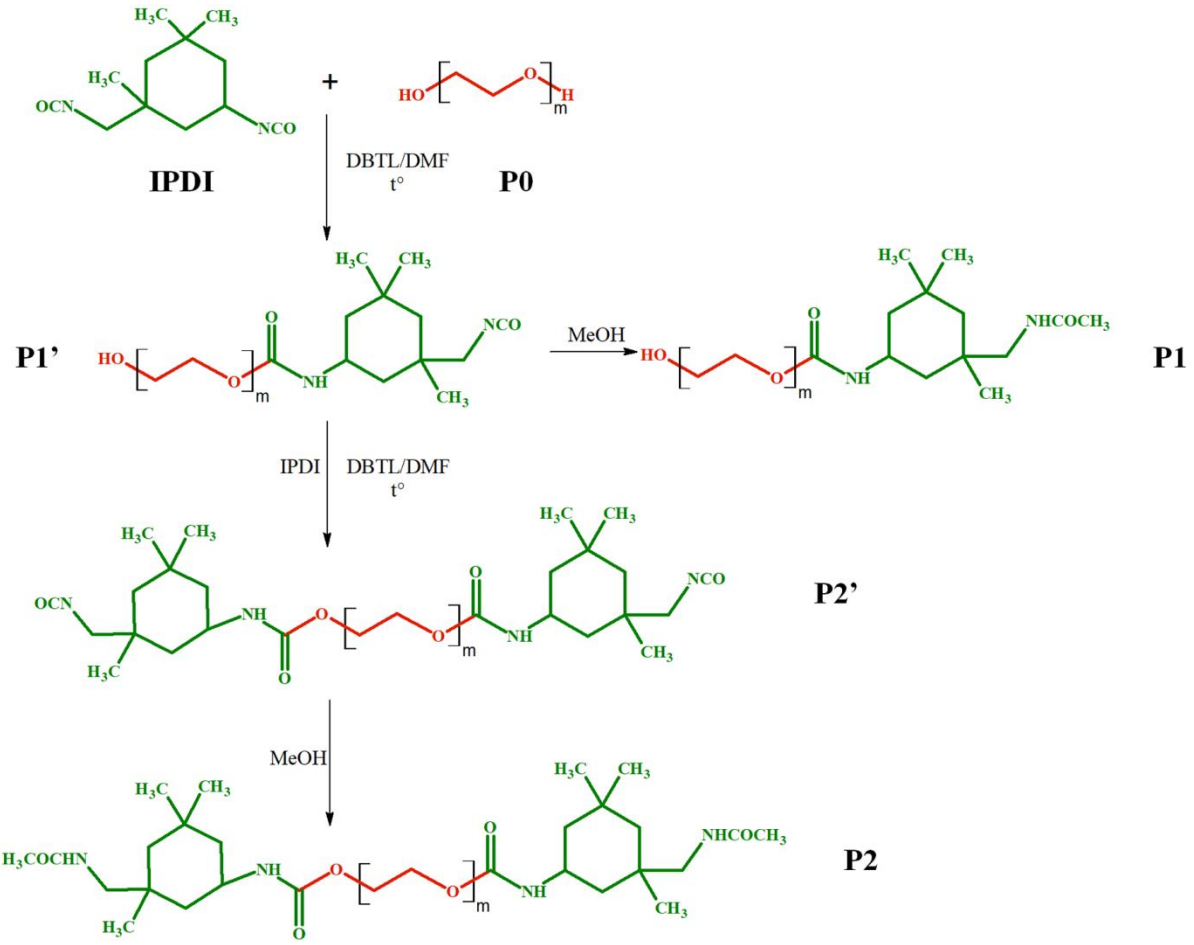


**Scheme 2.1**. Schematic representation of the formation of the reaction products analyzed by MALDI-MS

**Table 2.1.** Reaction conditions used to optimize the reaction between PEG and IPDI

| # | Temperature (°C) | Concentration (%)* | Molar ratio PEG/IPDI/DBTL | $k_{app}$ ($min^{-1}$)** |
|---|---|---|---|---|
| **1** | 35 | 15 | 1/2/0.018 | $1.13x10^{-2}$ |
| **2** | 35 | 30 | 1/2/0.018 | $3.81x10^{-2}$ |
| **3** | 35 | 5 | 1/2/0.018 | $0.29x10^{-2}$ |
| **4** | 35 | 15 | 1/2/0.054 | $1.59x10^{-2}$ |
| **5** | 50 | 15 | 1/2/0.018 | $2.75x10^{-2}$ |
| **6** | 25 | 15 | 1/2/0.018 | $0.09x10^{-2}$ |
| **7** | 35 | 15 | 1/2/0 | 0 |

* Calculated as the total content of reactants (IPDI, PEG, and DBTL) in the initial reaction mixture.
** Values calculated according to equation (12).

*2.2.1. Qualitative MALDI-MS analysis of PEG–IPDI prepolymers*

In **Figure 2.1a**, the signals in the MALDI-MS spectrum of the reactive sample collected from reaction **#2** (**Table 2.1**) show a main Gaussian distribution associated with three overlapping populations: unreacted PEG, mono-functionalized PEG, and di-functionalized PEG, denoted as P0, P1', and P2', respectively.

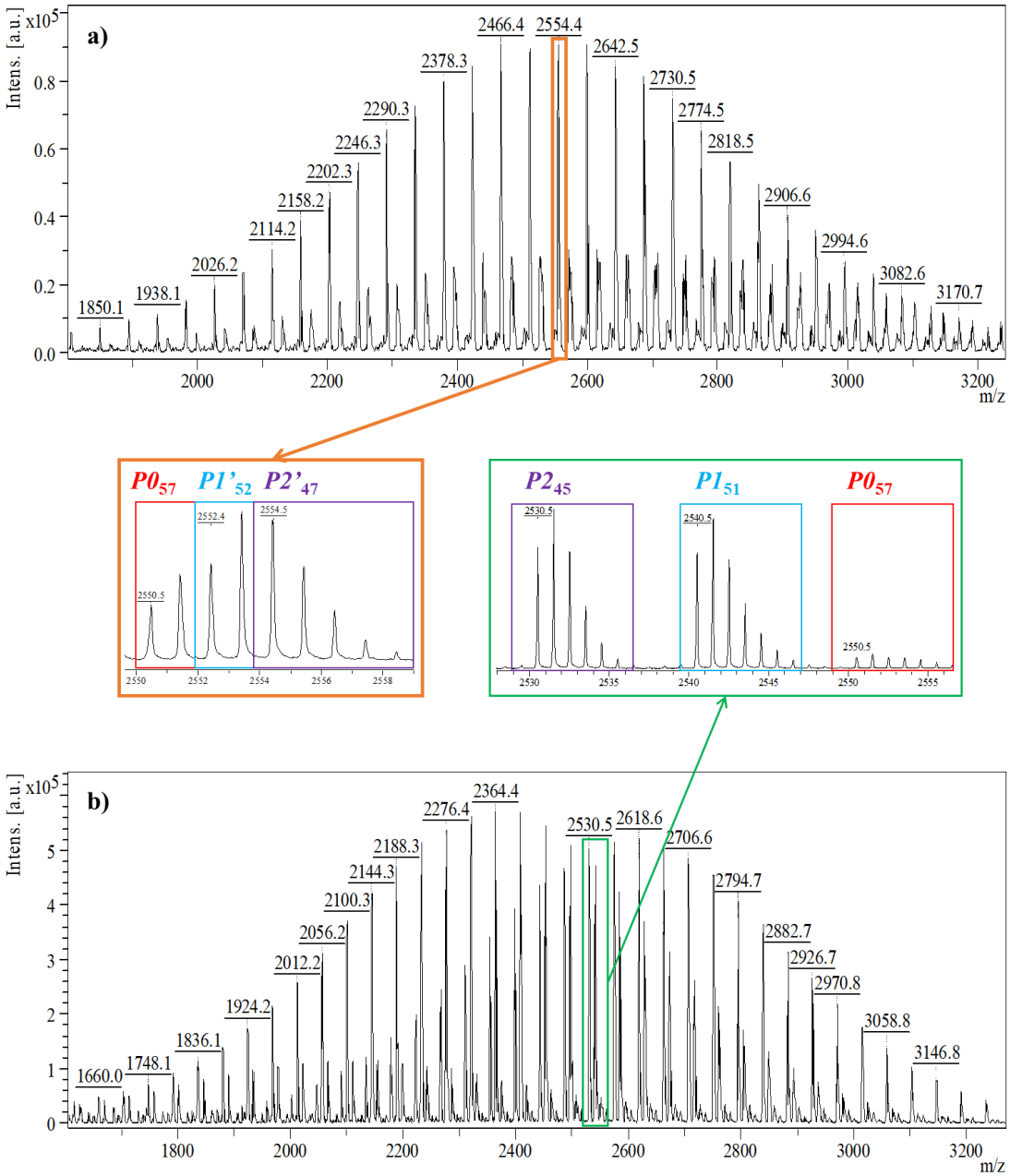


**Figure 2.1.** MALDI-MS spectra of (a) reactive compounds and (b) compounds with reactive chain ends blocked with MeOH from the reaction mixture obtained in reaction **#2** (**Table 2.1**) at 15 min. The indices associated with the symbols P0, P1, and P2 indicate the number of ethylene oxide units.

The highlighted signals in **Figure 2.1a** correspond to the sodium adduct of a difunctionalized PEG chain with n = 47 ethylene oxide monomer units (marked as $P2'_{47}$). In proximity, two additional signals—$P0_{57}$ and $P1'_{52}$—belong to other series. Due to the overlap of monoisotopic signals (**Figure 2.1a** – zoomed region), differentiating the signals from the P0, P1', and P2' series is difficult, and semi-quantitative analysis of the products cannot be performed.

On the other hand, the MALDI-MS spectrum of P0, P1, and P2 compounds recorded after blocking the NCO groups with MeOH (**Figure 2.1b**) shows a remarkable difference between the signals (enlarged region). The signals corresponding to the mono-functionalized and di-functionalized series are shifted by 32 Da (P1 series) and 64 Da (P2 series), respectively. Thus, derivatization with MeOH allows each population of P0, P1, and P2 compounds to be easily recognized and, importantly, quantitatively analyzed.

### *2.2.2. Quantitative MALDI-MS analysis of PEG–IPDI prepolymers*

The progress of PEG functionalization can be determined by considering all the signals in the MALDI-MS spectrum, associating the relative intensities in the MS spectra with their relative concentrations in the reaction mixture to calculate the number-average molecular weight (Mn) of each collected sample. The plot of Mn evolution over time highlights the point at which Mn reaches the theoretical value corresponding to difunctionalized PEG, as shown in **Figure 2.5a**.

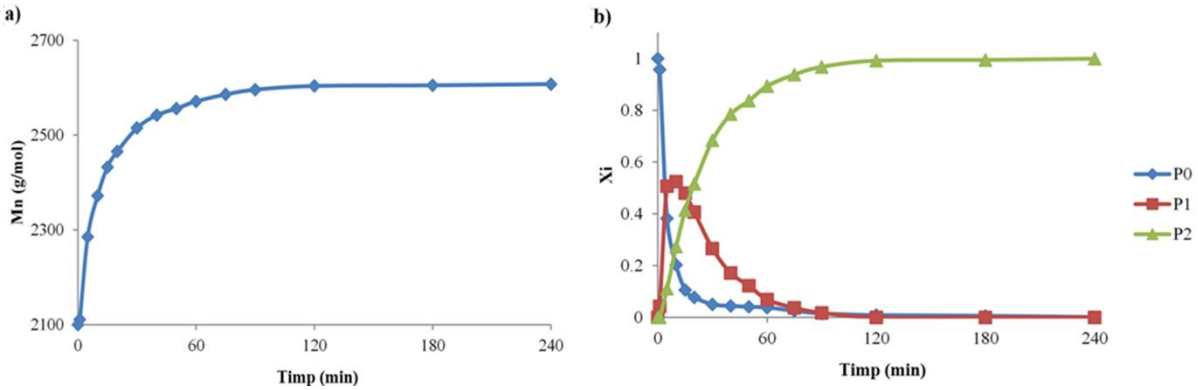


**Figure 2.5.** (a) Evolution of Mn and (b) evolution of each species type P0, P1, and P2.

The observed increase from 2100 g/mol to 2608 g/mol corresponds to the attachment of two IPDI molecules and two MeOH molecules to the ends of the PEG chains in the derivatized reaction mixture, $\Delta m = (2 \times 222 + 2 \times 32)$ g/mol = 608 g/mol. This approach is useful when analyzing and comparing reaction systems that reach complete conversion of the reactive species, which

represents the theoretical case. However, actual reaction conditions may lead to reduced conversion. In such situations, a more precise analysis would involve deconvolution of the overall Mn increase to observe the evolution of each chain type and quantify the relative amounts of P1 and P2 species (**Figure 2.5b**).

Analysis of the MALDI-MS oligomer fractions (**Figure 2.5b**) shows that the reaction of PEG with IPDI initially leads to a rapid decrease in P0 species, accompanied by the fast formation of P1 species, followed by a decrease in P1 as they are quickly converted into P2 species. This characterization method accurately reflects the evolution of the system and can be used to optimize reaction conditions.

2.2.2.2. Concentration influence

The effect of the total reactant concentration on the reaction between PEG and IPDI was studied for three different concentrations in DMF, and the evolution of the reaction mixture is shown in **Figure 2.8**. MALDI-MS kinetics revealed significant differences in the evolution of both P1 and P2 species as the total reactant concentration increased from 5% to 30%. For the reaction time considered in these syntheses (180 min), complete conversion of P1 species into P2 species was achieved in the case of the highest concentration (30%). Furthermore, it can be observed that the formation of P1 species occurs more rapidly at higher concentrations, and the rate of their consumption, due to the formation of P2 species, similarly depends on concentration.

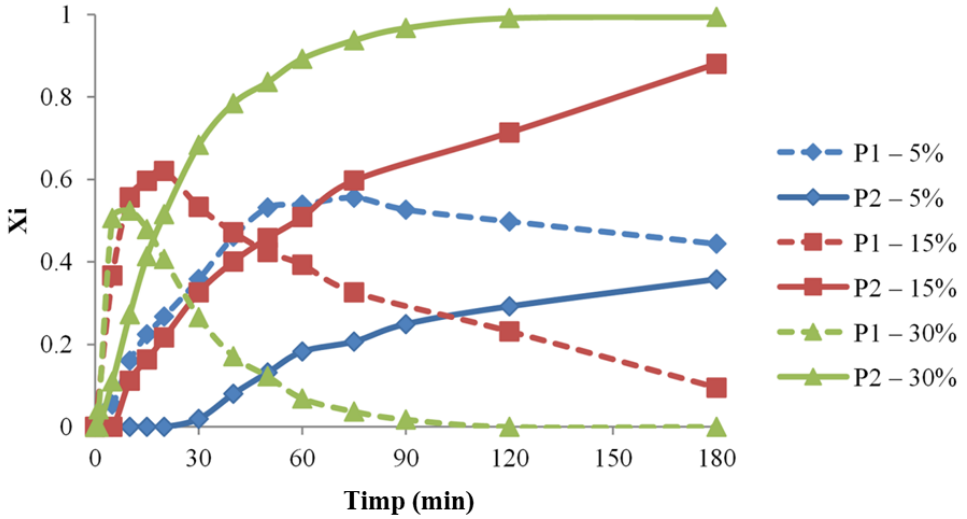


**Figure 2.8**. Evolution of the relative molar fractions of P1 and P2 species under different concentration conditions (reactions **#1, 2, 3** – **Table 2.1**)

### 2.3. Investigation of the formation of cyclodextrin-isophorone diisocyanate prepolymers

**Scheme 2.4** illustrates the reaction leading to the functionalization of β-CD with IPDI (CD–NCO). To prevent product modifications caused by side reactions before MALDI MS analysis, the CD–NCO product was subjected to an additional derivatization step, in which the reactive moieties were capped with MeOH (structure A, **Scheme 2.4**).

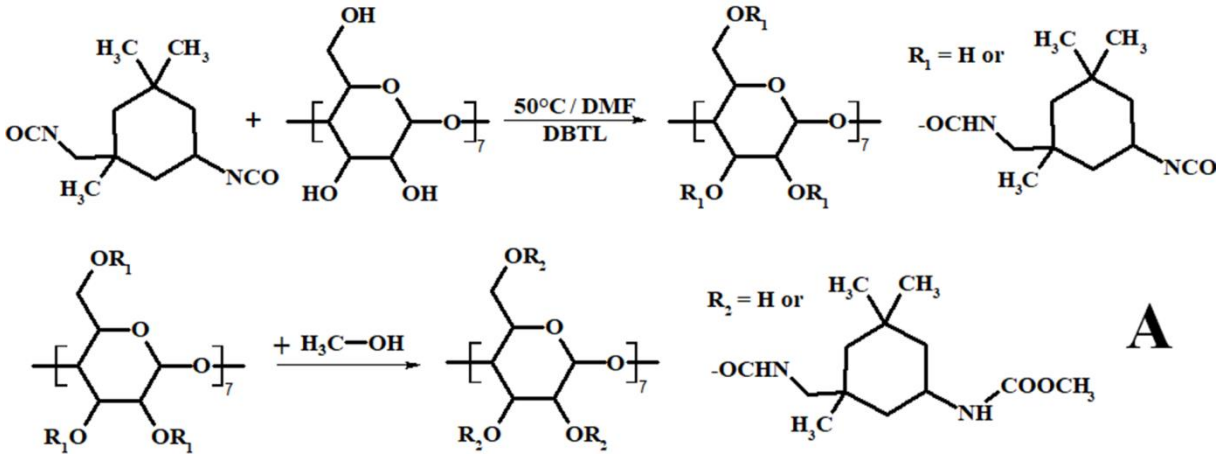


**Scheme 2.4.** Schematic representation of the reaction between CD and IPDI with the formation of the main product CD-NCO (structures A)

*2.3.1. Qualitative analysis by MALDI MS of CD-NCO derivatives*

The evolution of the CD–NCO compound, presented in **Figure 2.11**, indicates a steady increase in the substitution degree (GS), reaching up to four IPDI units per CD molecule. The MS signal corresponding to β-CD substituted with four IPDI units appears at m/z = 2174. However, at higher GS values, additional MS signals of lower intensity emerge alongside the main series, indicating the formation of side products. For instance, in the spectrum of the sample collected after 30 minutes, these secondary signals become more pronounced (**Figure 2.11**). These species are formed during the reaction and are subsequently revealed through MeOH derivatization.

Structures of types A–C correspond to CD–NCO molecules bearing a similar number of NCO functionalities but differing in their substitution patterns, either prior to or during MeOH derivatization. Type A represents the main CD–NCO product, with the signal at *m/z* = 2936 attributed to a β-CD molecule functionalized with seven IPDI units. Type B corresponds to a product in which one NCO group is no longer available for MeOH derivatization. This suggests that the missing NCO group has reacted with an OH group from the same CD molecule (**Scheme 2.6**, type B structure). In contrast, type C structures, which are 26 Da lower than the corresponding

B-series, result from the reaction of an NCO group with water, leading to the formation of $NH_2$ groups (**Scheme 2.6**, type C structure).

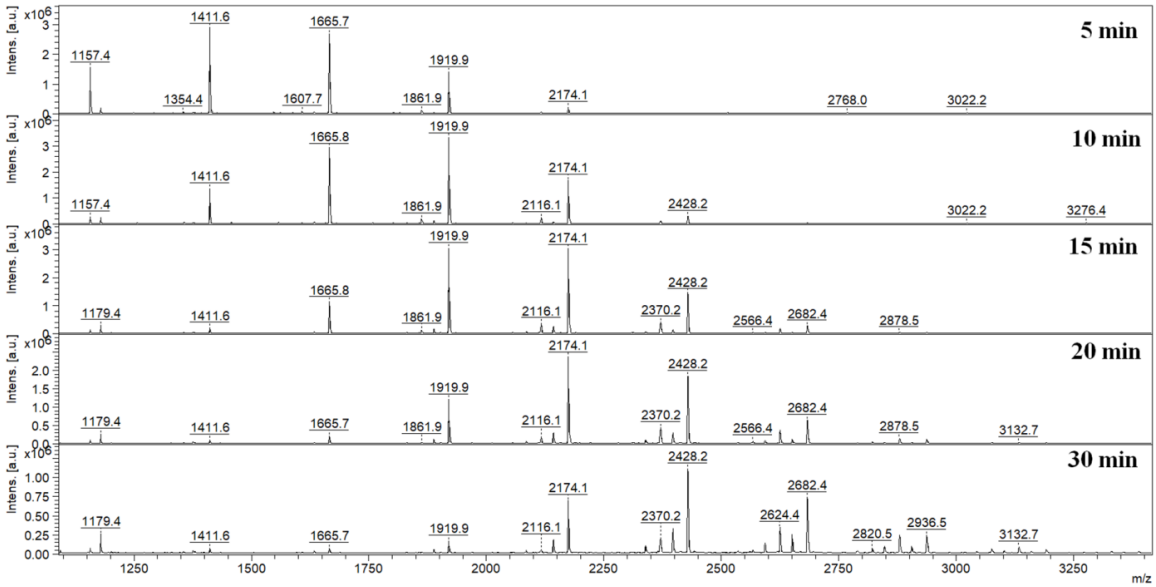


**Figure 2.11**. Evolution of the CD-NCO compound followed by MALDI MS for the reaction system performed at 15% percentage concentration and 1/20 molar ratio CD/IPDI

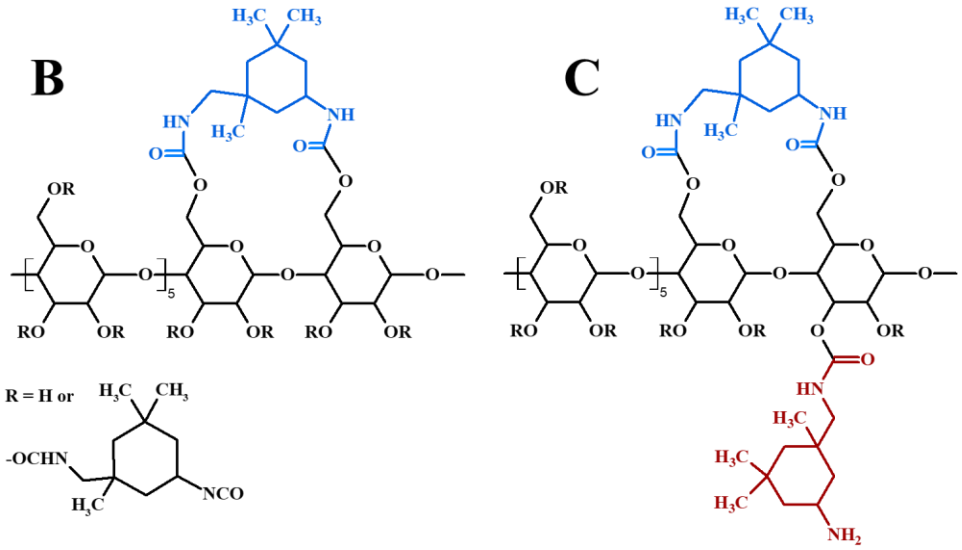


**Scheme 2.6.** Structures associated with type B and C structures observed from MALDI MS analysis

Overall, MALDI MS analysis of A–C-type structures reveals two secondary processes responsible for reducing the number of NCO groups available for further derivatization: intra/inter-cyclodextrin reactions and interactions with residual water.

*2.3.2. Quantitative analysis by MALDI MS of CD-NCO derivatives*

Following the MALDI MS characterization of CD–NCO products, further optimization of the β-CD substitution reaction with IPDI was established. Three reaction systems were investigated by varying the CD/IPDI molar ratio and the total concentration:

- **R1** – CD/IPDI ratio = 1:10, total concentration 5%
- **R2** – CD/IPDI ratio = 1:20, total concentration 5%
- **R3** – CD/IPDI ratio = 1:20, total concentration 15%

The average degree of substitution (GSm) was defined as the average number of IPDI units attached per CD molecule, taking into account not only the main products but also those arising from side reactions, as evidenced by the presence of B and C type structures in the MALDI MS spectra. GSm was calculated using the following relationship:

$$GS_m = \frac{\sum_{x=1}^{n} GS_x \times I_{px}}{\sum_{x=1}^{n} I_{px}} \quad (15)$$

where $GS_x$ is the degree of substitution corresponding to peak x, and $Ip_x$ is the intensity of that peak.

The comparative plot in **Figure 2.13a** shows that an excess of IPDI leads to an increase in GSm, as observed when comparing systems R1 and R2. Similarly, increasing the total concentration (R2 vs. R3) produces a comparable effect, resulting in higher GSm values. The highest GSm was obtained for system R3, reaching approximately four IPDI units per CD after 20 minutes of reaction.

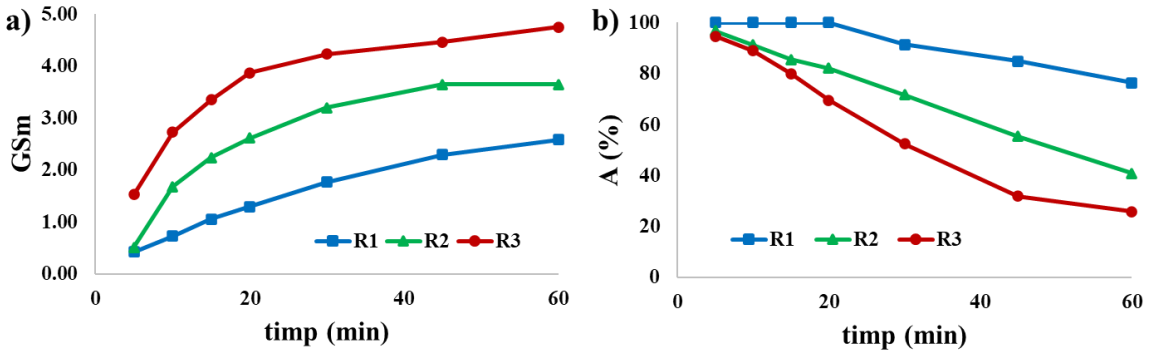


**Figure 2.13**. Influence of reaction parameters a) on GSm and b) substitution decay of the main product

However, GSm alone does not fully capture the impact of the side reactions described earlier. To better illustrate these effects, the evolution of NCO groups lost through intramolecular crosslinking

and hydrolysis (conversion to amines in the presence of residual water) was evaluated (**Figure 2.13b**). The influence of these secondary processes on GSm was quantified using a parameter called substitution decay (A), defined as the ratio between the cumulative intensity of peaks corresponding to type A structures and the total intensity of all detected peaks (types A–C):

$$\% \boldsymbol{A} = \frac{\sum_1^n \boldsymbol{I_p}}{\sum_1^n \boldsymbol{I_t}} \times \mathbf{100} \quad (16)$$

where $I_p$ represents the intensity of peaks associated with the main CD–NCO product, and $I_t$ includes all peaks in the spectrum, including those of secondary products.

As shown in **Figure 2.13b**, GSm impairment increases significantly with increasing concentration and decreasing CD/IPDI molar ratio. Moreover, analysis of the reaction conditions indicates that this impairment becomes more pronounced at higher GSm values. This trend is also evident in **Figure 2.11**, where an increase in both the number and relative intensity of MS signals corresponding to species with partially degraded NCO functionalities can be observed.

# CHAPTER 3. POLYURETHANE-CYCLODEXTRIN MODIFIED WITH OLIGOLACTIDE NANOPORROUS PARTICLES

## 3.2. Optimization of the crosslinking process between CDLA and IPDI compounds

For the synthesis of nanoporous particles (PNP), the concentration in DMF was initially varied, followed by the use of different molar ratios between CDLA derivatives (α-, β-, and γ-CDLA) and IPDI, as shown in **Table 3.1**. These variations in concentration and molar ratio were performed to determine the optimal synthesis conditions.

### *3.2.1. Influence of reactant concentration on the crosslinking reaction*

This experiment aimed to identify the optimal solvent amount required to obtain solid-state products, in which the reactant molecules are interconnected through covalent bonds, as a function of reaction yield. Four total concentrations of the reactant solutions in DMF were investigated (15%, 30%, 50%, and 70%, corresponding to reactions #**6–9 in Table 3.1**), using a fixed molar ratio of β-CDLA to IPDI of 1:10.

As indicated by the results presented in **Table 3.1**, only the syntheses performed at concentrations of 50% and 70% (reactions **#6** and **#9**) resulted in the formation of solid polymer networks. In contrast, at lower concentrations of 15% and 30% (reactions **#7** and **#8**), no solid products were

obtained. This can be attributed to inhomogeneous crosslinking, which hindered the formation of a continuous network throughout the reaction medium.

**Table 3.1**. Synthesis parameters used to obtain polyurethane PNPs

| # | CDLA tipe | Molar ratio CDLA:IPDI | Molar ratio OH:NCO | Concentration % | Yield % |
|---|---|---|---|---|---|
| **1** | α-CDLA | 1:2.5 | 18:5 | 50 | 87 |
| **2** | | 1:5* | 18:10 | 50 | 89 |
| **3** | | 1:10 | 18:20 | 50 | 90 |
| **4** | β-CDLA | 1:2,5 | 21:5 | 50 | - |
| **5** | | 1:5* | 21:10 | 50 | 91 |
| **6** | | 1:10 | 21:20 | 50 | 89 |
| **7** | | 1:10 | 21:20 | 15 | - |
| **8** | | 1:10 | 21:20 | 30 | - |
| **9** | | 1:10 | 21:20 | 70 | 79 |
| **10** | γ-CDLA | 1:2,5 | 24:5 | 50 | - |
| **11** | | 1:5* | 24:10 | 50 | 93 |
| **12** | | 1:10 | 24:20 | 50 | 90 |

*the product obtained was subsequently subjected to the mechanical grinding process

In other words, the high solvent content at lower concentrations limited the extent of crosslinking across the reaction mass, thereby preventing the formation of homogeneous, solid materials. Based on these findings and considering the obtained reaction yields, a total concentration of 50% was identified as optimal for the synthesis of PNP based on CDLA and IPDI.

*3.2.2. Influence of the CDLA/IPDI molar ratio on the crosslinking reaction*

Following the polyaddition reaction between the OH groups of CDLA and the NCO groups of IPDI, solid materials were obtained after purification. In the case of α-CDLA, homogeneous networks were formed for all molar ratios investigated. In contrast, for β- and γ-CDLA, network formation occurred only at molar ratios of 1:5 and 1:10 (CDLA to IPDI).

At a molar ratio of 1:2.5 for β- or γ-CDLA and IPDI (reactions **#4** and **#10**), a significant increase in the viscosity of the reaction medium was observed; however, this was not accompanied by effective crosslinking. After blocking the unreacted NCO groups with MeOH, a clear solution was obtained. This behavior indicates an incomplete crosslinking process, which failed to produce a

three-dimensional network, unlike in the case of α-CDLA. The insufficient number of NCO groups (**Table 3.1**) at a 1:2.5 molar ratio prevents the formation of interconnected 3D networks throughout the reaction mass. Therefore, the crosslinking of CDLA derivatives is strongly influenced by parameters such as concentration, OH/NCO molar ratio, and the type of CDLA derivative (α-, β-, or γ-CDLA).

### 3.4. Obtaining and characterizing nanoporous particles

The PNPs obtained after grinding exhibited a well-defined morphology (**Figure 3.7**). SEM analysis revealed structures with a slightly fusiform shape and a narrow size distribution. The particle sizes, resulting from the grinding process, were in the nanometer range (60–180 nm). The average particle diameter was similar for β- and γ-CDLA samples (approximately 111 nm), while slightly larger values were observed for α-CDLA particles (approximately 124 nm).

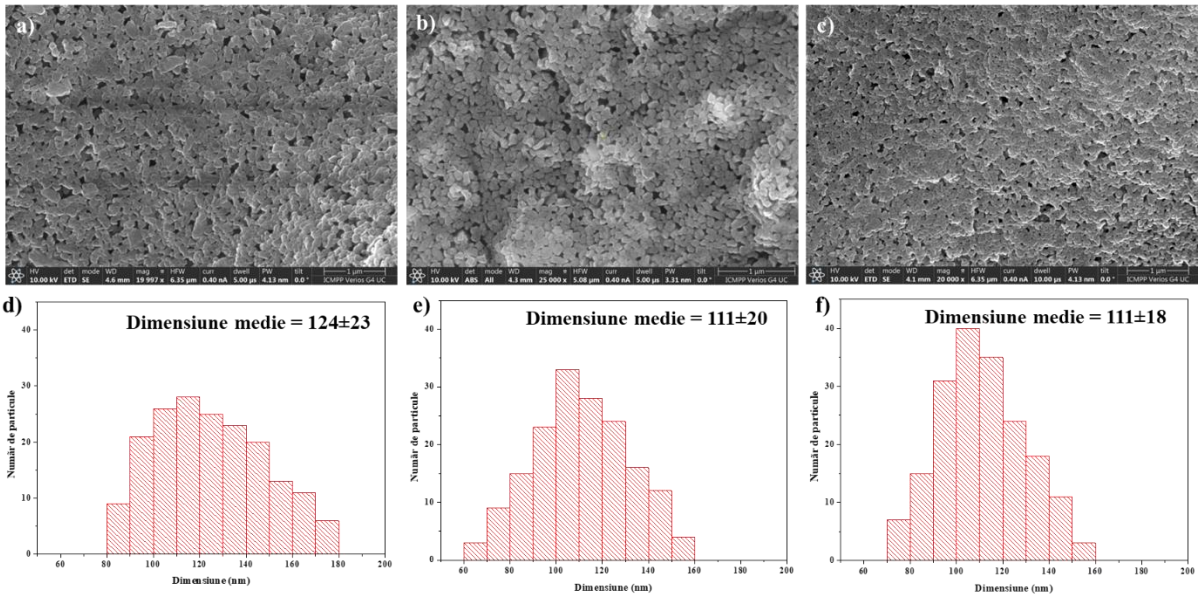


**Figure 3.7.** SEM images and particle size histograms of the products PNP-α-CDLA (a, d), PNP-β-CDLA (b, e), and PNP-γ-CDLA (c, f)

Solubility tests demonstrated that the PNPs are insoluble in water, methanol, ethanol, acetone, DMF, DMSO, and chloroform. However, they exhibit significant water uptake, with an absorption capacity of 230–280%. The synthesized materials display a negative zeta potential, indicating a negatively charged surface, likely due to the presence of CDLA hydroxyl groups. The specific surface area, determined by the BET (Brunauer–Emmett–Teller) method based on adsorption isotherms, ranges between 57 and 63 $m^2/g$. Particle size analysis by dynamic light scattering (DLS)

showed average values between 159 and 185 nm, which are consistent with the dimensions estimated from SEM measurements.

### 3.5. Absorption of dyes from aqueous media

The PNPs obtained after the grinding process were employed in sorption studies of the cationic dye Basic Blue 41 (BB41). The objective of these studies was to evaluate the sorption capacity of PNPs based on α-, β-, and γ-CDLA, to assess the influence of the cyclodextrin cavity on the absorption process, and to investigate the effects of initial dye concentration and contact time.

Initially, the sorption performance toward BB41 was evaluated for all three types of PNPs. Preliminary results (**Figure 3.9**) indicate that the sorption efficiency is strongly dependent on the type of CDLA incorporated into the polymer network. Among the tested materials, β-CDLA-based PNPs exhibited the highest performance (54 mg/g, corresponding to 90% removal), whereas significantly lower sorption capacities were observed for PNP-α-CDLA (30 mg/g, 50%) and PNP-γ-CDLA (28 mg/g, 47%). All systems showed rapid sorption kinetics, reaching values close to the equilibrium within the first 10 minutes.

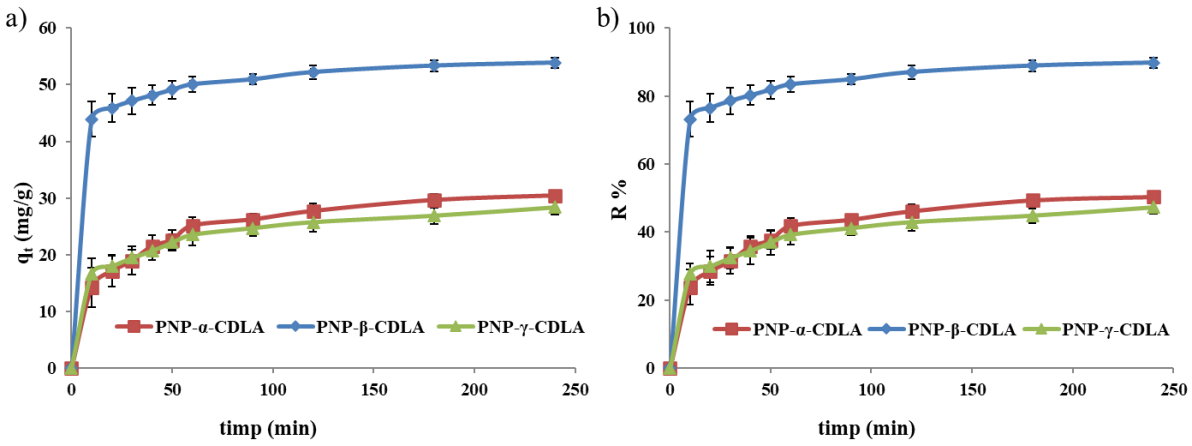


**Figure 3.9**. Comparative study of the three types of PNP: a) the amount of BB41 absorbed, and b) the percentage of removal using the dye concentration of 75 mg/L

These results suggest that PNPs containing β-CDLA possess superior sorption capacity, likely due to the optimal cavity size of β-CDLA. This cavity is larger than that of α-CDLA but smaller than that of γ-CDLA, making it particularly suitable for accommodating BB41 molecules and thereby enhancing sorption efficiency.

*3.5.1. BB41 dye absorption kinetics*

Further investigations on BB41 sorption were conducted using PNP-β-CDLA particles at four different initial dye concentrations (25–100 mg/L). The effect of initial concentration on the sorption process is presented in **Figure 3.10**. The results demonstrate that PNP-β-CDLA exhibits high sorption capacity toward BB41. After 10 minutes of contact, a substantial fraction of the dye was removed (approximately 86% at the lowest initial concentration, C0 = 25 mg/L; **Figure 3.10a**).

As shown in **Figure 3.10b**, increasing the initial dye concentration leads to a decrease in removal efficiency (from 86% to 64%). The sorption process is rapid, and extending the contact time results in only a modest increase in removal efficiency (approximately 10%). These findings indicate that a minimum contact time of 10 minutes is sufficient for significant dye removal using PNP-β-CDLA.

Overall, BB41 sorption occurs rapidly, with maximum sorption capacity reached after approximately 60 minutes, confirming strong interactions between the dye molecules and the polymer network of the PNPs.

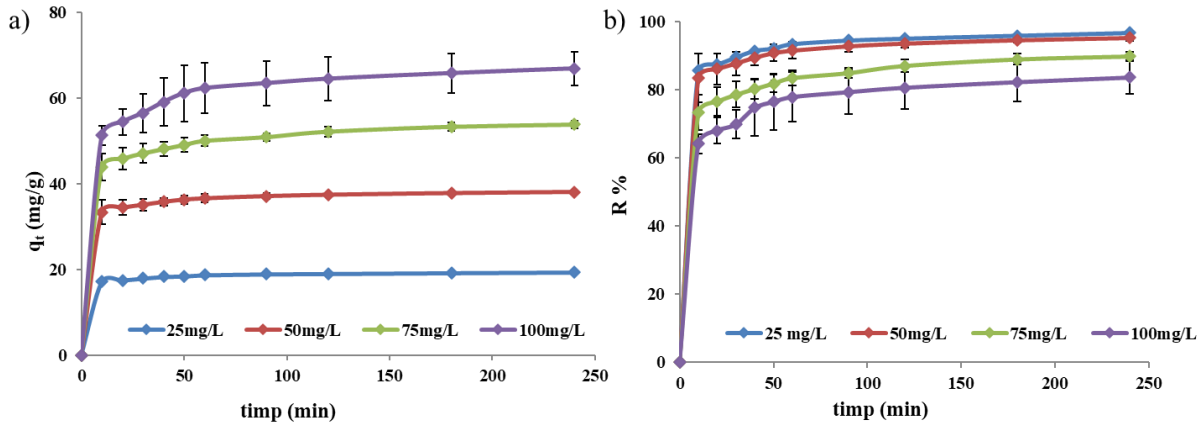


**Figure 3.10**. Equilibrium studies of a) the amount of absorbed BB41 and b) the BB41 removal capacity at different initial concentrations (C1=25 mg/L, C2=50 mg/L, C3=75 mg/L and C4=100 mg/L) of the PNP-β-CDLA sample

The graphical representations of the pseudo-first-order (PFO) and pseudo-second-order (PSO) kinetic models are presented in **Figure 3.11**. The PSO model shows a significantly better fit to the experimental data, as indicated by the higher correlation coefficients ($R^2$ = 0.9988–0.9998) and lower relative error values (RE between −8% and 4%), compared to the PFO model ($R^2$ = 0.7408–0.855; RE between 69% and 82%). Furthermore, the equilibrium adsorption capacities ($q_e$)

calculated using the PSO model closely match the experimental values. These findings suggest that the sorption process follows PSO kinetics, indicating strong interactions between the adsorbent and dye molecules, potentially associated with chemisorption mechanisms.

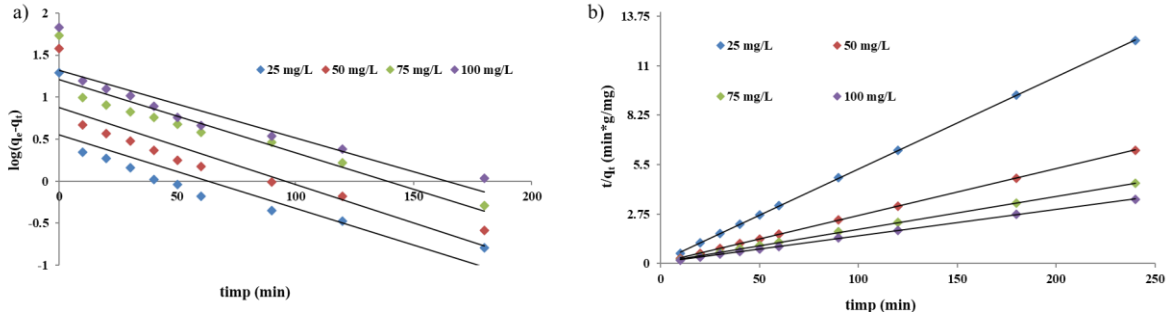


**Figure 3.11**. a) Pseudo-first-order kinetics and b) pseudo-second-order kinetics

*3.5.2. Absorption isotherms*

Adsorption isotherms provide important information regarding the sorption capacity and the distribution of dye molecules between the solid and liquid phases. To evaluate the adsorption behavior of PNP-β-CDLA, the two most widely used models—Langmuir and Freundlich—were applied (**Figure 3.12**).

The adsorption equilibrium data for BB41 are best described by the Langmuir model, as evidenced by the high correlation coefficient ($R^2 = 0.9966$). This suggests that the adsorption process occurs on a homogeneous surface, forming a monolayer of adsorbed molecules without interactions between adsorbed species. According to the Langmuir model, the maximum adsorption capacity ($q_m$) is 76.34 mg/g, which is in good agreement with the experimentally determined value (66.87 mg/g).

To further elucidate the nature of the adsorption process (i.e., physical adsorption, ion exchange, or chemisorption), the Dubinin–Radushkevich (D–R) isotherm model was employed (**Figure 3.12**). The calculated mean free energy (E = 4.08 kJ/mol) indicates that the sorption process is predominantly governed by physical interactions between the dye molecules and the adsorbent. Additionally, the maximum adsorption capacity estimated using the D–R model (66.22 mg/g) is very close to the experimental value obtained at the highest dye concentration ($q_e$ = 66.87 mg/g).

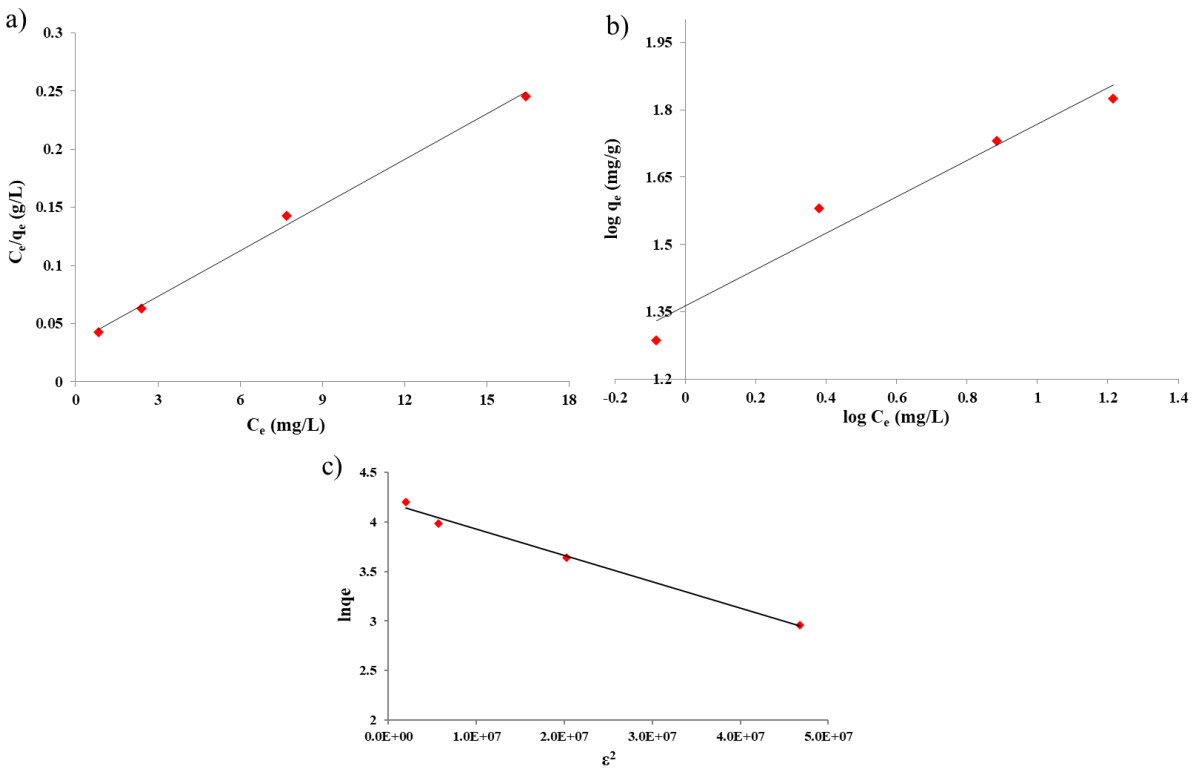


**Figure 3.12**. a) Langmuir, b) Freundlich and c) Dubinin-Radushkevich isotherms of BB41 absorption on PNP

*3.5.4. Reusability of nanoporous particles*

Following dye saturation, the material was successfully regenerated using MeOH as the desorption solvent. Five consecutive adsorption–desorption cycles were performed, and the results are shown in **Figure 3.14a**. The material demonstrated excellent regeneration capability, with nearly complete dye desorption observed in each cycle.

A slight decrease in adsorption capacity was observed after the first cycle, from 62 mg/g to 56 mg/g, although the desorption efficiency remained unaffected. In subsequent cycles (2–5), only minor reductions in adsorption capacity (2–3 mg/g) were recorded. The initial decrease suggests that a small fraction of dye molecules remained trapped within the material, possibly due to steric hindrance within the cyclodextrin cavities or the network structure. However, from the second cycle onward, this effect was no longer significant, and complete desorption was achieved after MeOH treatment.

The consistent and reproducible results obtained after the second cycle indicate stable sorption performance and good chemical stability of the material under the applied experimental conditions. These findings confirm the potential for practical reuse of the adsorbent.

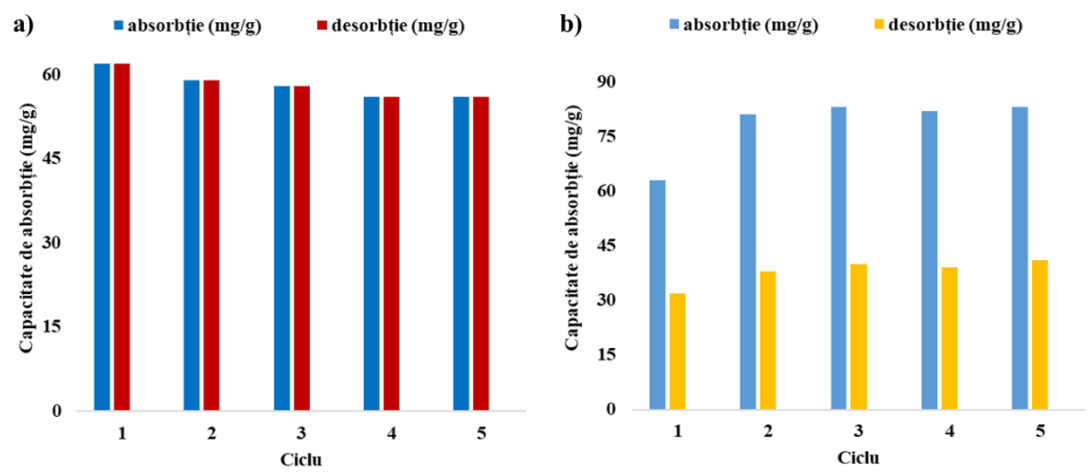


**Figure 3.14**. Graphical representation of the absorption capacity of PNP-β-CDLA for five consecutive absorption-desorption cycles using (a) MeOH and (b) a mixture of MeOH and acetic acid

In a separate adsorption–desorption experiment, a mixture of MeOH and acetic acid (0.1 M) in a volumetric ratio of 9:1 was used as the desorption solvent. After the first adsorption–desorption cycle, the sample exhibited similar adsorption behavior; however, only approximately half of the absorbed dye was released during desorption (**Figure 3.14b**).

During cycles 2–5, the sample showed an increased adsorption capacity compared to the first cycle (up to 82 mg/g), but still failed to achieve complete dye desorption. These results indicate that this solvent mixture is not effective for full dye removal. However, the presence of acetic acid appears to modify the interaction mechanism between PNP-β-CDLA and BB41.

A possible explanation for these observations involves partial degradation of the PNP-β-CDLA network under acidic conditions, likely through hydrolytic cleavage of the oligolactide bridges. This degradation may lead to the formation of additional interstitial spaces, thereby enhancing the adsorption capacity. Simultaneously, acetic acid may promote partial dissociation of BB41 and facilitate its retention within the polymer network, contributing to the incomplete desorption observed.

### *3.5.5. Absorption mechanism*

The PNP-β-CDLA material contains multiple active sites for dye adsorption, including the cyclodextrin cavities and the intermolecular linkages between CD and IPDI. Following the grinding process, structural and surface modifications occurred, leading to the formation of negatively charged regions, as evidenced by the negative zeta potential. The cationic dye BB41

can interact with these sites through electrostatic attractions, as well as through hydrogen bonding and van der Waals interactions.

Although the PSO kinetic model suggests strong interactions between the adsorbent and the dye, the mean free energy value obtained from the Dubinin–Radushkevich model indicates that the process is predominantly governed by physical adsorption mechanisms. These include hydrogen bonding, van der Waals interactions, and inclusion complex formation within the cyclodextrin cavities.

# CHAPTER 4. POLYURETHANE-β-CYCLODEXTRIN MODIFIED WITH OLIGOESTERS HYDROGELS

## 4.2. Investigation of β-CD-, β-CDLA-, and β-CDCL–PEG polyurethane networks

To further investigate the influence of hydroxyl group type on the polyaddition reaction, both native and modified β-cyclodextrins were studied. Native β-CD contains seven primary hydroxyl groups (OH-P) and fourteen secondary hydroxyl groups (OH-S). Two modified derivatives were also considered: oligolactide-modified β-CD (β-CDLA), in which primary hydroxyl groups are partially esterified and converted into secondary hydroxyl groups, and oligocaprolactone-modified β-CD (β-CDCL), where secondary hydroxyl groups are partially esterified and converted into primary hydroxyl groups.

The evolution of the crosslinking reaction between β-CD, β-CDLA, or β-CDCL and PEG-$(NCO)_2$ prepolymers was subsequently investigated (**Scheme 4.1**).

### *4.2.2. Synthesis of β-CD-, β-CDLA- and β-CDCL-PEG polyurethane networks*

Three types of polymer networks containing native β-CD, β-CDLA, and β-CDCL were synthesized in order to highlight the differences arising during the crosslinking reaction of compounds with varying ratios of secondary (OH-S) and primary (OH-P) hydroxyl groups. The polyurethane networks were obtained via the crosslinking reaction (**Scheme 4.1**) between native (series B) or modified β-CD (series G for β-CDLA and series C for β-CDCL) and PEG-$(NCO)_2$ in DMF solution at 50 °C, at a total concentration of 34%, using DBTL as catalyst. The reaction parameters, including the type of hydroxyl-containing compound and the molar ratios of the reactants, are summarized in **Table 4.1**.

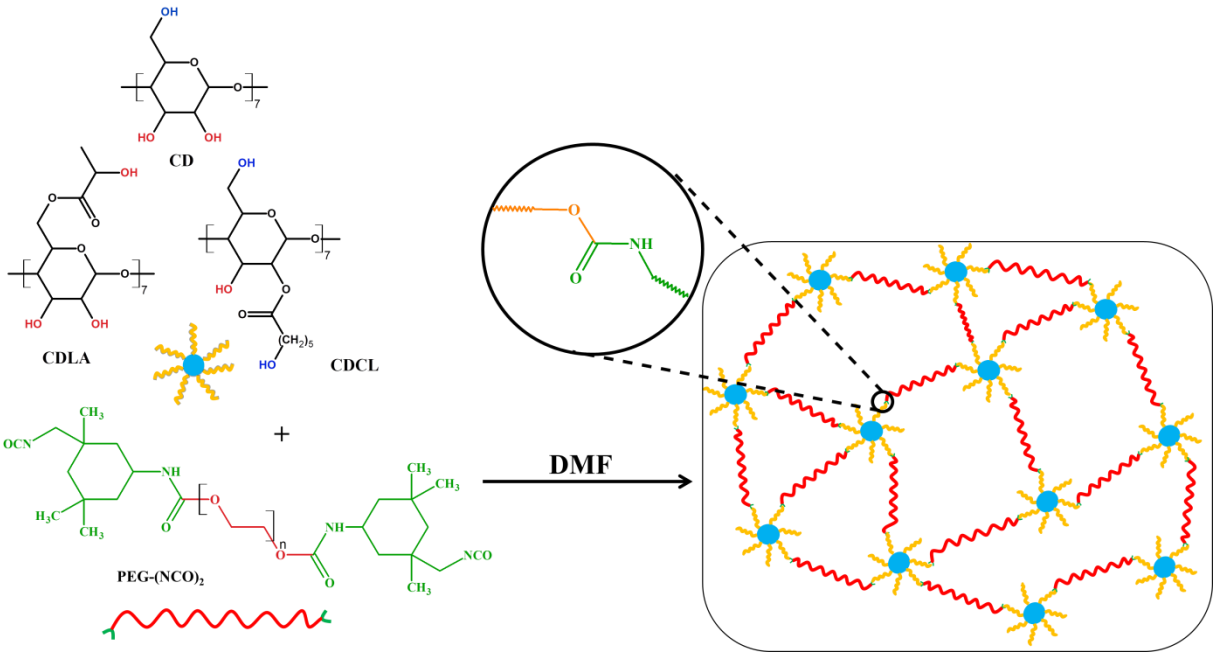


**Scheme 4.1**. Schematic representation of the formation of polyurethane networks

**Table 4.1.** Synthesis parameters

| # | Sample | Molar ratio | | | Molar ratio OH/NCO | yield, η % |
|---|---|---|---|---|---|---|
| | | β-CD: PEG-$(NCO)_2$ | β-CDLA: PEG-$(NCO)_2$ | β-CDCL: PEG-$(NCO)_2$ | | |
| **1** | **B4** | 1:4 | - | - | 21:8 | 97 |
| **2** | **B8** | 1:8 | - | - | 21:16 | 95 |
| **3** | **B12** | 1:12 | - | - | 21:24 | 93 |
| **4** | **G1** | - | 1:1 | - | 21:2 | - |
| **5** | **G2** | - | 1:2 | - | 21:4 | - |
| **6** | **G4** | - | 1:4 | - | 21:8 | 94 |
| **7** | **G8** | - | 1:8 | - | 21:16 | 91 |
| **8** | **G12** | - | 1:12 | - | 21:24 | 82 |
| **9** | **C2** | - | - | 1:2 | 21:4 | 96 |
| **10** | **C4** | - | - | 1:4 | 21:8 | 95 |
| **11** | **C8** | - | - | 1:8 | 21:16 | 97 |
| **12** | **C12** | - | - | 1:12 | 21:24 | 96 |

The integrity of the resulting networks was found to depend strongly on the molar ratio between the hydroxyl-bearing oligosaccharide component (β-CD, β-CDLA, or β-CDCL) and the PEG-diisocyanate prepolymer. Networks prepared with β-CDLA at molar ratios of 1:1 and 1:2 relative to PEG-$(NCO)_2$ (samples **#4** and **#5**, **Table 4.1**) exhibited an inhomogeneous structure, indicative of an incomplete or defective crosslinking process. In the case of networks G1 and G2, an increase

in the viscosity of the reaction mixture was observed; however, the resulting materials were mechanically unstable and prone to rupture during handling.

This behavior can be attributed to the predominance of less reactive OH-S groups, which leads to structural defects in the network, combined with an insufficient number of isocyanate groups required to form a fully interconnected three-dimensional structure throughout the reaction mass. In contrast, the use of β-CDCL resulted in the formation of a compact and homogeneous network at a molar ratio of 1:2 (sample **#9-C2, Table 4.1**). Although the OH/NCO ratio is identical for samples G2 and C2 (**#5-G2** and **#9-C2**), the network obtained with β-CDCL exhibited superior structural integrity. This can be explained by the higher content of reactive OH-P groups in β-CDCL compared to β-CDLA.

*4.2.3. Rheological study of reactions to obtain polyurethane networks*

The rheological behavior of the three series of crosslinking systems (based on native β-CD, β-CDLA, and β-CDCL) is presented in **Figure 4.11**, highlighting their characteristic gelation profiles. A clear dependence of gelation time on the chemical nature and composition of the reacting species can be observed.

For the β-CD-based systems (series B), the gelation time increases with increasing β-CD content, following the order: $T_{B12} < T_{B8} < T_{B4}$ (**Figure 4.11a**). This behavior can be explained by the fact that systems with a lower concentration of hydroxyl groups require less time for their incorporation into the three-dimensional network, leading to faster gelation through polyaddition reactions.

A similar trend was observed for systems containing β-CDLA (series G) and β-CDCL (series C), where the crosslinking reaction proceeded more rapidly at lower contents of β-CDLA or β-CDCL in the initial mixture ($T_{G12} < T_{G8} < T_{G4}$ and $T_{C8} < T_{C4} < T_{C2}$). These results indicate that, regardless of the type of cyclodextrin derivative used, an excess of isocyanate groups accelerates the consumption of hydroxyl groups and, consequently, the overall polyaddition process.

However, when comparing the B, G, and C series at similar molar ratios between the total number of hydroxyl and isocyanate groups, the gelation times of G series are significantly longer. For instance, in the case of network G4, gelation begins considerably later than in B4, and this trend is consistent across all corresponding G/B pairs. In contrast, the gelation times of series C are comparable to those of series B, the primary difference between these systems being associated with the nature of the hydroxyl groups involved.

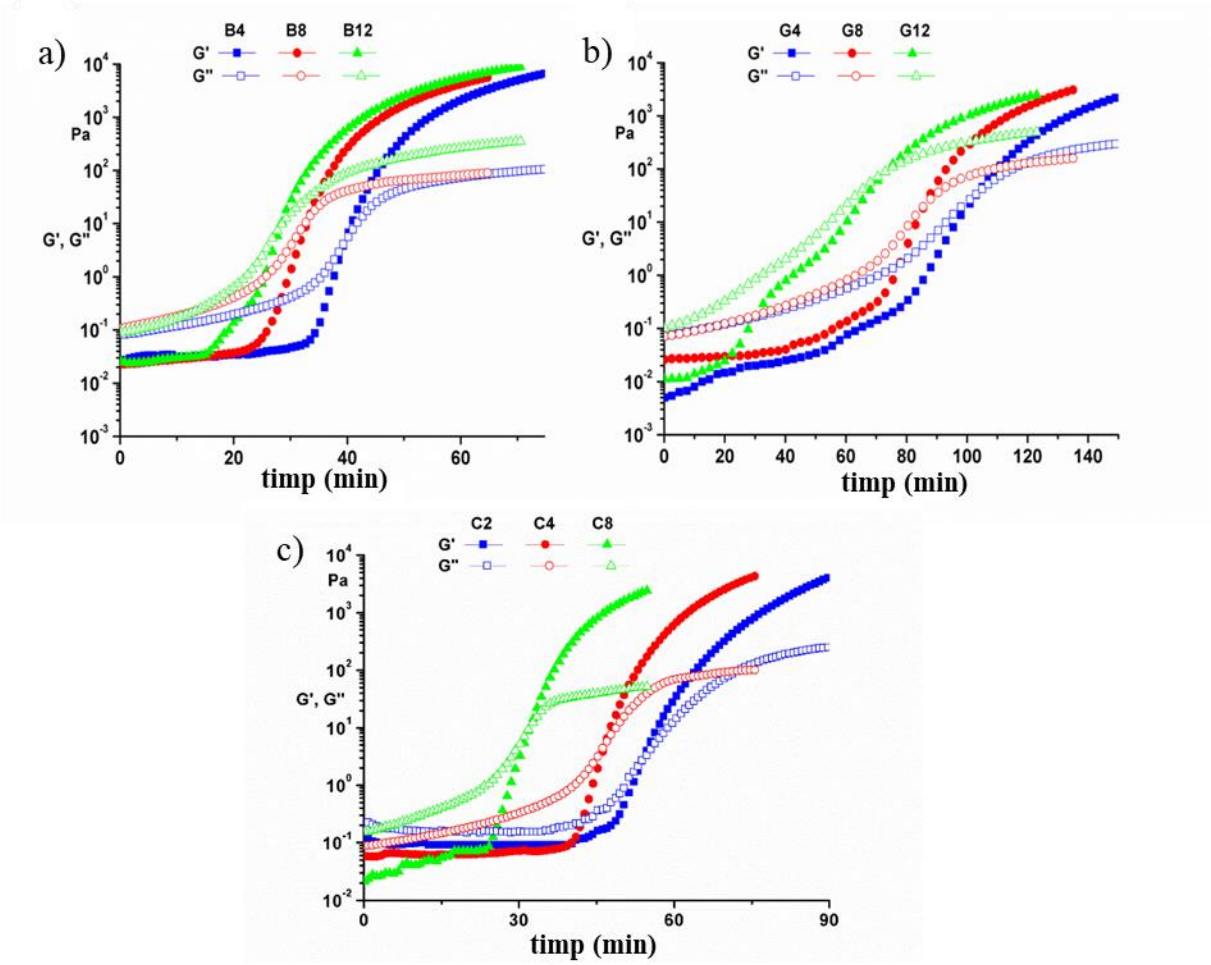


**Figure 4.11**. Representation of the G' and G" modulus versus time of networks based on a) native β-CD, b) β-CDLA, and c) β-CDCL

*4.2.5 Hydrolytic degradation study of polyurethane networks*

4.2.5.1. Hydrolytic degradation of β-CDLA-PEG networks

The incorporation of oligolactide (OLA) sequences into the crosslinked networks imparts hydrolytic degradability. The mass loss observed during hydrolytic degradation of β-CDLA–PEG hydrogels is presented in **Figure 4.18**, alongside data for a non-degradable β-CD–PEG hydrogel used as a reference under identical conditions (PBS buffer, pH = 7.4, 37.5 °C). The reference sample exhibited negligible mass loss, whereas the G series showed degradation profiles dependent on the OLA content of each sample. This confirms that degradation occurs primarily through hydrolysis of ester bonds, as expected.

The highest mass loss was observed for the G4 hydrogel, reaching approximately 48% after 193 days, while the sample with lower OLA content (G12) exhibited a mass loss of only about 20%.

Furthermore, all G-series hydrogels display a two-stage degradation profile: an initial rapid mass loss followed by a slower, more gradual phase. The first stage extends up to approximately 9 days for G4 and G8, and up to 18 days for G12. This behavior suggests that the degradation rate can be tuned by adjusting the β-CDLA content in the synthesis mixture.

The rapid initial mass loss is likely associated with the removal of more accessible OLA–PEG chains that are loosely connected to the network, possibly through a single chain end. Additionally, β-CDLA molecules with limited network integration may be released during this stage. The second, slower phase corresponds to the progressive degradation of the network structure, accompanied by diffusion-controlled removal of water-soluble degradation products.

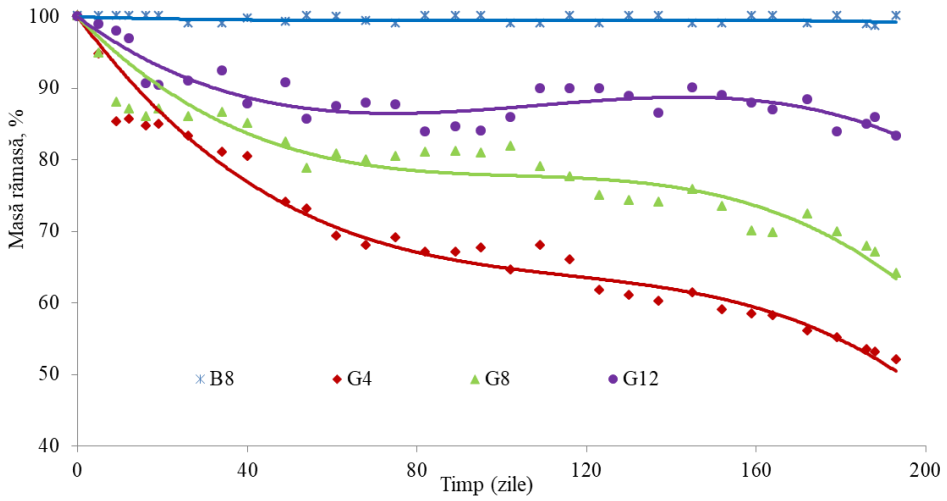


**Figure 4.18.** Graphical representation of mass loss due to hydrolytic degradation

The degradation process was further investigated by SEM analysis of samples collected after 9, 89, and 193 days. Pore formation was correlated with the mass loss profile by examining the morphology at different degradation stages. After 9 days, large pores with a broad size distribution (50–500 µm) were observed. At 89 days, the pore size distribution became narrower, and regions with lower porosity were still present. These observations indicate structural heterogeneity in G4 hydrogels, likely resulting from irregular crosslinking (**Figure 4.20**).

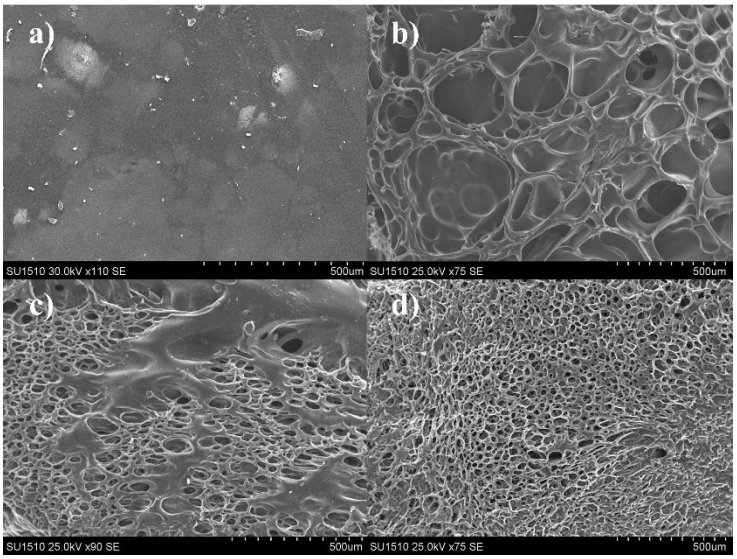


**Figure 4.20**. Surface SEM images of sample G4: a) initial, b) after 9 days, c) after 89 days, and d) after 193 days of degradation

SEM images obtained after 193 days of degradation further reveal the structure evolution, with a relatively small decrease in pore size and the disappearance of non-porous regions, resulting in a fully porous hydrogel. The pore diameters ranged from 5 to 50 μm (**Figure 4.20d**). Although the overall porosity appeared relatively homogeneous, suggesting bulk degradation, the presence of pores with different orientations indicates the persistence of macrostructural defects.

4.2.5.2. Hydrolytic degradation of β-CDCL-PEG networks

The incorporation of oligocaprolactone (OCL) sequences into the crosslinked networks also imparts hydrolytic degradability. It is important to note that, compared to oligolactide (OLA), OCL undergoes degradation at a significantly slower rate [380]. Consequently, the hydrolytic degradation behavior of the prepared hydrogels was investigated under accelerated conditions in a basic medium.

Mass loss measurements for the β-CDCL–PEG series revealed comparable degradation profiles, as shown in **Figure 4.23**. Hydrogels C4–C12 exhibited a gradual and continuous decrease in mass, correlated with the β-CDCL content in the system. In contrast, sample C2, which contains the highest amount of β-CDCL, showed rapid degradation, with approximately 60% residual mass remaining after 1 day, followed by complete dispersion in the degradation medium after 3 days.

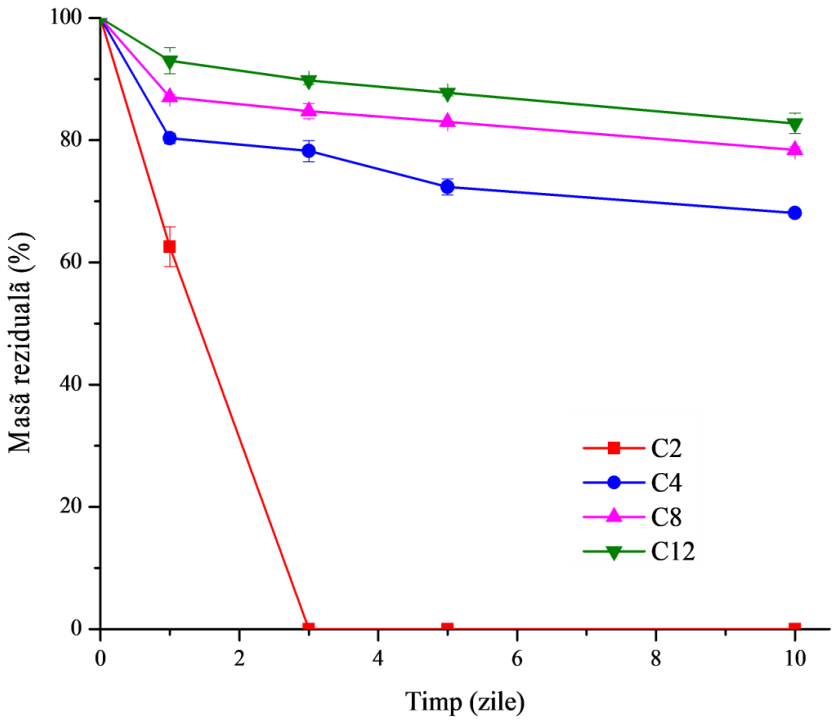


**Figure 4.23.** Graphical illustration of the mass loss profiles of C2, C4, C8 and C12 during degradation

Samples C4, C8, and C12 displayed a more controlled degradation behavior, with continuous mass loss throughout the investigated period. After 10 days, the residual mass values were approximately 68%, 78%, and 83%, respectively.

Morphological changes during the degradation process were investigated by SEM analysis. For sample C2 (**Figure 4.24**), the initial surface appeared relatively smooth, with slight roughness (**Figure 4.24a**). After 24 hours (**Figure 4.24b**), significant structural disintegration was observed, accompanied by substantial mass loss and the formation of large pores. The degradation process led to a complete transformation of the material, from a flexible hydrogel to a fragile, thin structure that was difficult to handle, ultimately resulting in full dispersion in the aqueous medium.

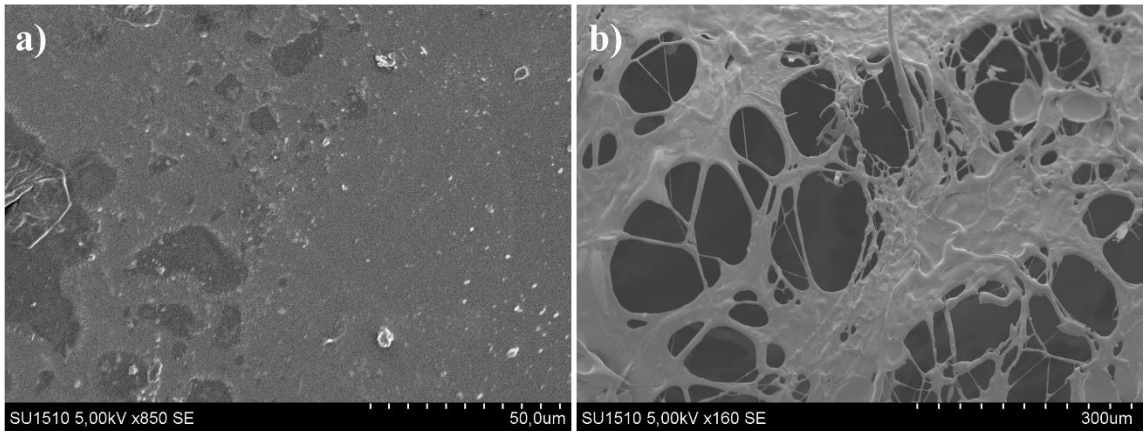

**Figure 4.24**. Surface SEM micrographs of sample C2: a) initial and b) after 1 day of degradation

In contrast, the degradation of sample C4 occurs predominantly at the surface, as evidenced by SEM micrographs obtained from cross-sectional analysis (**Figure 4.25**). No significant structural changes or pore formation were observed within the bulk of the material. However, the surface underwent progressive degradation, characterized by the formation and growth of pores over time, up to 5 days of exposure. After 10 days, surface images revealed the disappearance of pores and the formation of protuberances (**Figure 4.25d**).

This behavior suggests that the surface layer of the material is gradually eroded, exposing microphases that are more resistant to degradation than the surrounding matrix. Surface erosion could be attributed to a diffusion gradient of water, leading to preferential accumulation at the surface, as reported for certain hydrophobic materials [381,382]. However, swelling experiments (*subchapter 4.2.6*) demonstrated that all hydrogels, including C4, swell uniformly without macroscopic discontinuities, indicating a relatively homogeneous distribution of water throughout the material. Therefore, preferential surface accumulation of water can be considered negligible in this case.

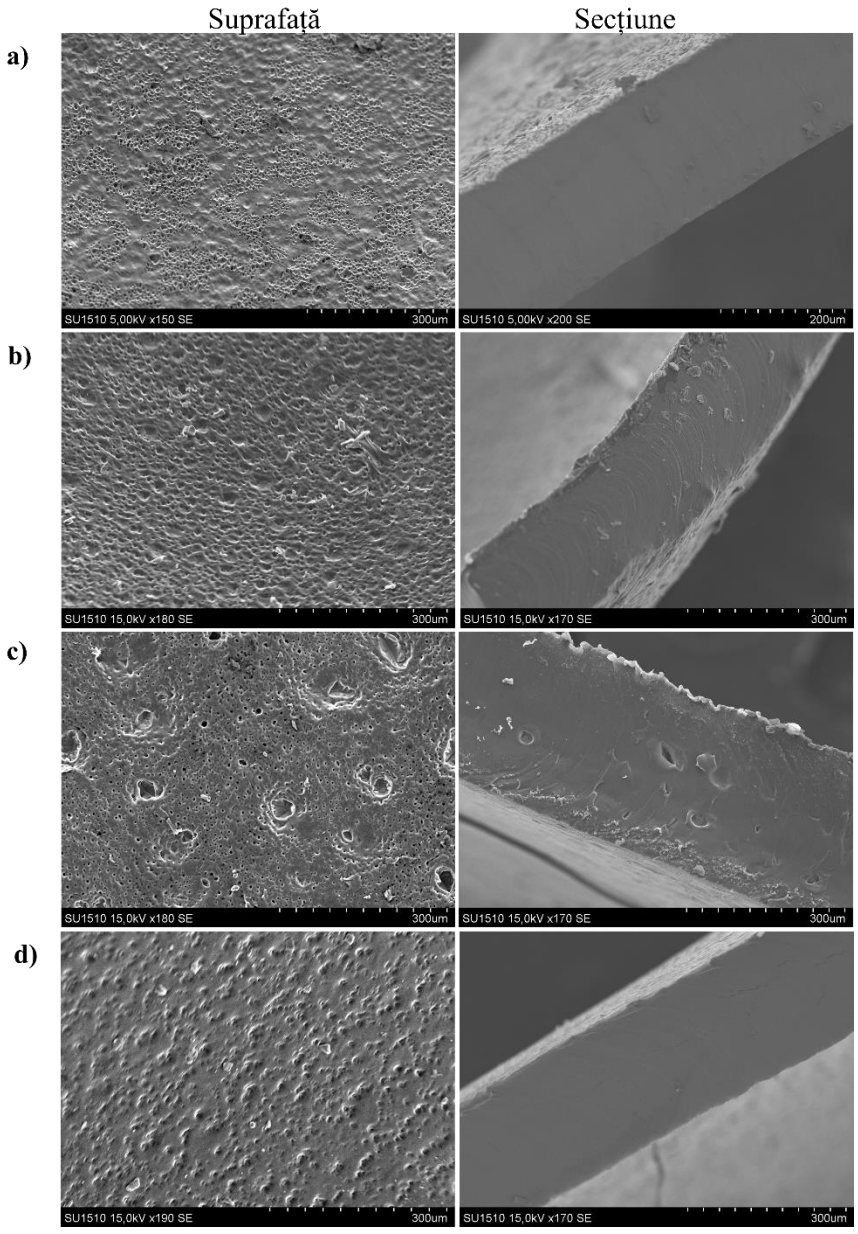


**Figure 4.25.** SEM micrographs of sample C4 after a) 1 day, b) 3 days, c) 5 days, and d) after 10 days of degradation

*4.2.6. Swelling in water and release of levofloxacin*

The initial investigation also focused on the interaction between water and the β-CD–PEG, β-CDLA–PEG, and β-CDCL–PEG hydrogels (**Figure 4.28**). For series B (**Figure 4.28a**), the β-CD content had only a minor influence on the swelling degree, with relatively small differences in water uptake.

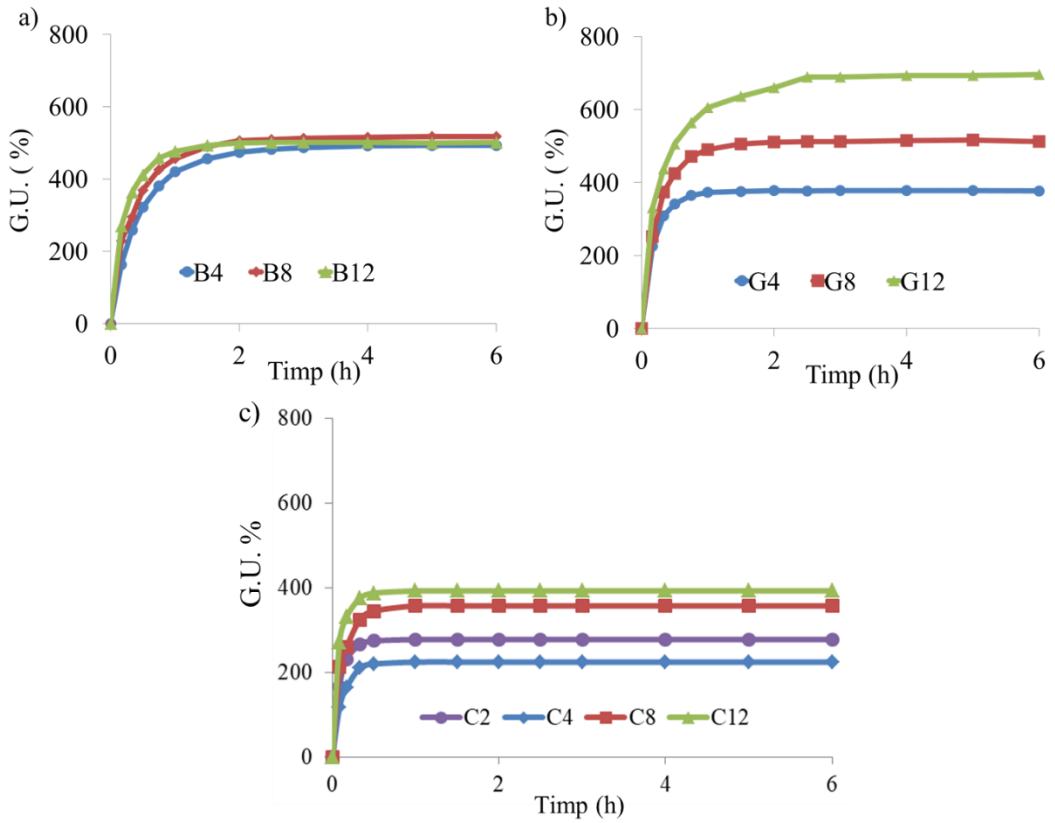


**Figure 4.28**. Swelling degree of hydrogels: a) β-CD-PEG, b) β-CDLA-PEG and c) β-CDCL-PEG

In contrast, the G series exhibited a distinct swelling behavior (**Figure 4.28b**), where decreasing the β-CDLA content in the reaction mixture led to a significant increase in water absorption, from approximately 350% (G4) to 700% (G12). This trend can be attributed to the increased homogeneity of hydroxyl group distribution, which promotes more regular network packing compared to the B series.

For the C series (**Figure 4.28c**), samples C4–C12 showed an increasing swelling degree from approximately 200% to nearly 400%, representing the lowest water uptake among the studied systems (maximum swelling degree, GUmax ≈ 400% for C12). This behavior can be explained by the presence of hydrophobic OCL segments within the hydrogel structure. Additionally, the higher proportion of primary hydroxyl groups promotes the formation of more tightly crosslinked networks, resulting in a more compact structure.

Among the investigated materials, β-CDCL–PEG hydrogels were selected for further evaluation as potential drug delivery systems, primarily due to their lower swelling capacity. The release

efficiency of LEV (**Figure 4.29b**) ranged from 81% for sample C4 to 91% for sample C12. Although the variation in release efficiency is relatively small (approximately 10%), the release follows the same increasing trend as the swelling degree (C4 < C2 < C8 < C12).

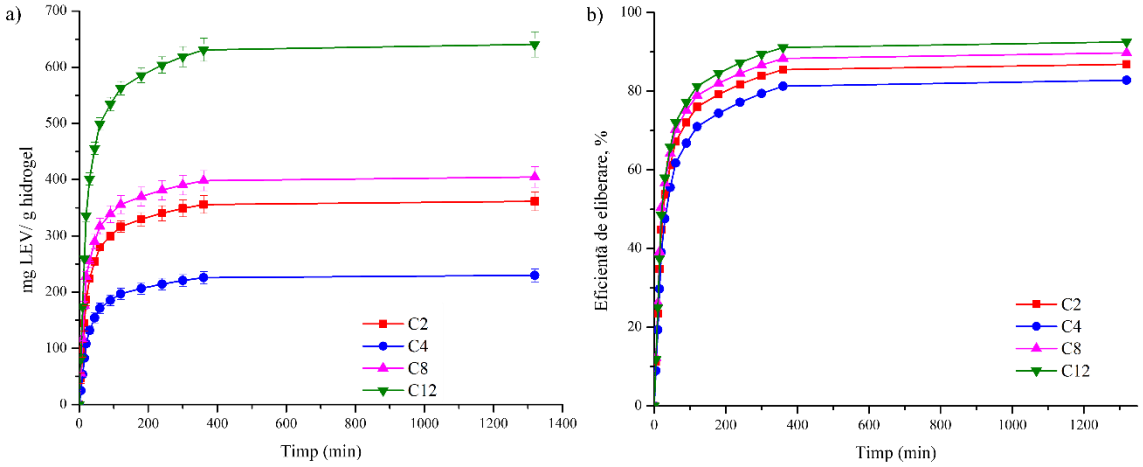


**Figure 4.29**. Amount of a) LEV release and b) release efficiency

Overall, the incorporation and release of LEV from the hydrogel network appear to be influenced by its solubility in water, as well as by the structural and swelling characteristics of the polymer network.

## GENERAL CONCLUSIONS

The main objective of this thesis was the development, optimization, and characterization of biodegradable polymer–cyclodextrin crosslinked systems, obtained in the form of gels or particles through polyaddition reactions between esterified cyclodextrins (CDs) and diisocyanate monomers or diisocyanate-based macromers. These systems were designed for potential applications in dye adsorption and the controlled release of active compounds.

The originality of this research, compared to similar studies reported in the literature, lies in two key aspects: the use of cyclodextrins esterified with oligoesters and the advanced analytical techniques employed. In particular, structural characterization of prepolymers by MALDI-MS enabled precise and efficient optimization of the reaction systems. Furthermore, the correlation between the properties of the synthesized materials and the structure of the starting compounds

was achieved by monitoring the evolution of the polyaddition reactions through dynamic rheological measurements.

The research was organized into three experimental chapters, each contributing progressively to the overall objective, moving from simpler model systems to more complex structures.

In **Chapter 2,** the influence of key reaction parameters—such as concentration, temperature, and catalyst—on the synthesis of isocyanate-terminated prepolymers was investigated using two model systems: PEG–IPDI and β-CD–IPDI. In the PEG–IPDI system, prepolymers functionalized with terminal isocyanate groups were synthesized via the polyaddition of PEG hydroxyl groups with IPDI isocyanate groups. The synthesis of the PEG-$(NCO)_2$ prepolymer was optimized through a kinetic study monitored by MALDI-MS. This approach enabled the evaluation of the effects of reaction temperature, reagent concentration, and catalyst amount on product formation. Based on these results, the optimal synthesis conditions were identified as a reaction temperature of 50 °C and a total concentration of 30%. In the case of the β-CD–IPDI system, both isocyanate-functionalized β-CD prepolymers and secondary products were obtained. The latter resulted from intermolecular interactions between functionalized β-CD molecules or from intramolecular reactions that reduced the number of available NCO groups in the final prepolymer. MALDI-MS analysis provided insight into the influence of reaction parameters, such as total concentration and β-CD/IPDI molar ratio, on the average degree of substitution of the resulting products. The experimental results demonstrated that a molar ratio of CD/IPDI = 1:20, combined with a total concentration of 15% and a reaction time of 60 minutes, leads to the formation of a CD–NCO prepolymer with an average of 4.75 NCO groups per β-CD molecule. Overall, MALDI-MS proved to be a powerful tool for both qualitative and quantitative monitoring of the reaction products, enabling detailed structural elucidation and the identification of optimal synthesis conditions for obtaining the desired species.

**Chapter 3** focused on the synthesis and characterization of nanoporous particles (PNPs) based on α-, β-, and γ-CDLA crosslinked with IPDI. The influence of both reactant concentration and the OH/NCO molar ratio on the polyaddition reaction was systematically investigated. The formation of crosslinked networks was found to be strongly dependent on the balance between hydroxyl and isocyanate groups, with an excess of OH groups leading to incomplete crosslinking. The structure of the optimized materials (obtained at 50% concentration and a CDLA:IPDI molar ratio of 1:5) was confirmed by FTIR and TGA analyses. Subsequent mechanical processing by ball milling

yielded submicron particles with a narrow size distribution. The resulting PNPs exhibited particle sizes ranging from 60 to 180 nm, with an average diameter of approximately 111 nm, a BET surface area between 57 and 63 $m^2/g$, and a negative zeta potential. Adsorption studies using the cationic dye BB41 demonstrated superior performance for β-CDLA-based systems compared to those containing α- or γ-CDLA, emphasizing the importance of selecting an appropriate cyclodextrin type for targeted applications. The adsorption kinetics followed a pseudo-second-order (PSO) model, while the equilibrium data were best described by the Langmuir isotherm, indicating a homogeneous adsorption process involving monolayer coverage of the nanopore surfaces. The mean adsorption energy (E = 4.08 kJ/mol), calculated using the Dubinin–Radushkevich model, suggests that the process is predominantly governed by physical interactions, such as hydrogen bonding and van der Waals forces, consistent with inclusion complex formation between the dye molecules and cyclodextrin cavities. Thermodynamic parameters (negative ΔG and ΔH, and positive ΔS) further confirm the spontaneous and exothermic nature of the adsorption process. Moreover, the materials retained high adsorption efficiency over five successive adsorption–desorption cycles, demonstrating good reusability. Hydrolytic degradation studies revealed that the internal surface area of the PNPs could be increased up to 160 $m^2/g$, highlighting the advantage of incorporating esterified cyclodextrins in the design of such materials.

**Chapter 4** addressed the synthesis of polyurethane hydrogels based on β-CD, β-CDLA, and β-CDCL, leading to the development of hydrolytically degradable materials. The results demonstrated, for the first time, that the evolution of crosslinking reactions can be controlled by considering the nature of hydroxyl groups present in the cyclodextrin derivatives. The reaction between NCO groups of PEG-$(NCO)_2$ and hydroxyl groups of β-CD derivatives was found to depend strongly on the predominant type of OH functionality. Thus, in β-CDLA systems, where secondary hydroxyl groups dominate, the crosslinking process proceeds more slowly, whereas in β-CDCL systems, characterized by a higher proportion of primary hydroxyl groups, the reaction occurs more rapidly. It was also established that network formation requires minimum molar ratios of 1:4 for β-CDLA:PEG-$(NCO)_2$ and 1:2 for β-CDCL:PEG-$(NCO)_2$. The network structure and connectivity were further investigated through hydrolytic degradation studies. Gravimetric analysis revealed degradation behaviors dependent on the type of ester bonds present. SEM analysis showed that β-CDLA–PEG hydrogels undergo bulk degradation with pore formation

throughout the material, whereas β-CDCL–PEG systems degrade predominantly via surface erosion. These findings demonstrate that the biodegradation profile can be tailored through the appropriate selection of oligoester-modified cyclodextrins. Furthermore, β-CDCL–PEG hydrogels were identified as promising candidates for controlled drug delivery applications. The release mechanism was found to follow a Super Case-II transport model, associated with enhanced mobility of PEG chains within the polymer network.

Overall, the results of this thesis demonstrate that careful selection of cyclodextrin structure, reaction conditions, and functionalization strategies enables precise control over the physicochemical properties of polymer–cyclodextrin conjugates. These findings contribute original insights into the design and application of polyaddition-based functional materials, supporting their potential use in fields such as environmental remediation and controlled delivery of active compounds.

The original contributions of this work have been disseminated through 4 published ISI-indexed articles (cumulative impact factor: 14.4), 8 oral presentations, and 3 poster presentations at national and international conferences.

## DISSEMINATION OF RESULTS AND OTHER SCIENTIFIC ACTIVITIES

**Papers published in ISI-listed scientific journals (results included in the thesis)**

1. **A.-D. Diaconu,** M. Balan-Porcarasu, V. Harabagiu, C. Peptu. The investigation of β-cyclodextrin derivatization with isophorone diisocyanate through MALDI mass spectrometry, Revue Roumaine de Chimie 2025, 70(7-8), 455-463. (FI ISI: 0,6)
2. **A.-D. Diaconu**, C.-L. Logigan, C.A. Peptu, C. Ibanescu, V. Harabagiu, C. Peptu. Polyurethane Degradable Hydrogels Based on Cyclodextrin-Oligocaprolactone Derivatives, Gels 2023, 9, 755. (FI ISI: 5,3)
3. D.-A. Blaj, **A.-D. Diaconu**, V. Harabagiu, C. Peptu. Polyethylene Glycol-Isophorone Diisocyanate Polyurethane Prepolymers Tailored Using MALDI MS, Materials 2023, 16 (2), 821. (FI ISI: 3,2)
4. C. Peptu, **A.-D. Diaconu**, M. Danu, C.A. Peptu, M. Cristea, V. Harabagiu. The Influence of the Hydroxyl Type on Crosslinking Process in Cyclodextrin Based Polyurethane Networks, Gels 2022, 8, 348. (FI ISI: 5,3)

**Papers published in ISI-listed scientific journals (results not included in the thesis)**

1. A.I. Barzic, **A.-D. Diaconu**, B.-C. Condurache, M. Soroceanu, R.M. Albu, I. Stoica. Assessment of optical and thermal properties of polyimide/metal oxide composites for photovoltaic uses, Bulletin of Materials Science, 2023, 46, 18. (FI ISI: 2,1)

**Papers published in journals at conferences (not included in the thesis)**

1. A.I. Barzic, R.M. Albu, M. Soroceanu, **A.-D. Diaconu**, B.-C. Condurache, I. Stoica. Effect of the dianhydride moieties on refraction properties of polyimides based on chalcogen elements, Tehnomus Journal - New Technologies and Products in Machine Manufacturing Technologies 2021, 69-73.

**Participation in national and international scientific events (results included in thesis)**

**a. Oral communications**

1. M. Cristea, D. Ionita, **A.-D. Diaconu**, C. Peptu. Understanding the evolution of the viscoelastic properties with temperature in cyclodextrin based polyurethane networks, PolyChar World Forum on Advanced Materials 30th Edition, Iași, România, 11-13 September 2024.
2. M. Cristea, D. Ionita, **A.-D. Diaconu**, C. Peptu. Molecular mobility phenomena in cyclodextrin-based polyurethane networks studied by dynamic mechanical analysis, IUPAC Macro 2024, the 50th World Polymer Congress, Coventry, United Kingdom, 1-4 July 2024.
3. **A.-D. Diaconu**, D.-A. Blaj, V. Harabagiu, C. Peptu. Harnessing MALDI mass spectrometry technique for tailored polyurethane prepolymers, XXXIIIth edition of the International Congress of "Apollonia" University of Iasi, Iași, 2-5 March 2023.
4. **A.-D. Diaconu,** M. Danu, M. Cristea, V. Harabagiu, C. Peptu. Impact of cyclodextrin derivatives' structure on the polyurethane crosslinking reaction and network properties, ICMPP – Open door to the future, MacroYouth2022, Iași, 18 noiembrie 2022.
5. **A.-D. Diaconu**, M. Danu, V. Harabagiu, C. Peptu. OH type influenced crosslinking for the control of swelling properties in CD-PEG/polyurethane networks, The XXXIIth edition of the International Congress of "Apollonia" University of Iasi, 28 February-2 March 2022.
6. M. Cristea, D. Ionita, **A.-D. Diaconu**, C. Peptu. How oligolactide moiety influences the molecular mobility of β-cyclodextrin polyurethane hydrogels: DMA and DSC investigations. The 47$^{th}$ North American Thermal Analysis Society Conference, Virtual Conference, 3-6 August 2021.

7. **A.-D. Diaconu**, V. Harabagiu, C. Peptu. Cyclodextrin-oligolactide polyurethane hydrogels,The XXXIth edition of the International Congress of "Apollonia" University of Iasi, 1-3 March 2021.
8. **A.-D. Diaconu**, V. Harabagiu, C. Peptu. Polyurethane degradable hydrogels, ICMPP – Open door to the future, MacroYouth2020, Iași, 19 Noiembrie 2020.

**b. Posters**

1. M. Cristea, D. Ioniță, **A.-D. Diaconu**, C. Peptu. Cyclodextrin-based polyurethane networks: Temperature dependent viscoelastic properties monitored by dynamic mechanical analysis, International Congress on Rheology, Athens, Greece, 29 iulie-4 august 2023.
2. **A.-D. Diaconu**, C. Peptu, V. Harabagiu. Degradable hydrogels based on cyclodextrin-polyurethane, The Silesian Meetings on Polymer Materials POLYMAT 2022, Zabrze, Poland, 17 March, 2022
3. **A.-D. Diaconu**, C. Peptu, V. Harabagiu. Cyclodextrin-polyurethane degradable hydrogels, The 4$^{th}$ International EPNOE Junior Scientist Meeting, Online Meeting, 3-4 February, 2021

**Participation in national and international scientific events (results not included in the thesis)**

1. I. Stoica, I. Sava, I. Butnaru, A. I. Barzic, R. M. Albu, C. Ursu, M. Asandulesa, **A.-D. Diaconu**. Properties of supramolecular polyimide/azodye systems configurated to be employed as flexible base layer for printed electronics, International Antalya Scientific Research and Innovative Studies Congress-III, Antalya, Turcia, 13-14 februarie 2023.
2. I. Stoica, E.-L. Epure, A.I. Barzic, M. Asandulesa, C. Ursu, I. Mihaila, **A.-D. Diaconu**, I. Sava. Physical and chemical properties of cyano-containing polyimide/azo-chromophore systems designed for flexible electronic products, International Colloquium "Physics of Materials" – PM 7, București, România, 10-11 noiembrie 2022.
3. R.M. Albu, M. Soroceanu, **A.-D. Diaconu**, B.-C. Condurache, I. Stoica, A.I. Barzic. Metal oxide filled polyimides for photovoltaics shielding, the 2$^{ND}$ International Antalya Scientific Research and Innovative Studies Congress, Antalya, Turkey, 17-21 March 2022.
4. A.I. Barzic, R.M. Albu, M. Soroceanu, **A.-D. Diaconu**, B.-C. Condurache, I. Stoica. Effect of the dianhydride moieties on refraction properties of polyimides based on chalcogen elements, The 21th International Scientific Conference „TEHNOMUS", Virtual Conference, 12 November 2021.

**Research projects (team member)**

1. *Design of cyclodextrin-polyester-amides for special applications* (Proiect de schimburi interacademice dintre Academia Română (ICMPP, Iași) și Academia de Științe a Poloniei (Centre of Polymer and Carbon Materials Polish Academy of Sciences, Zabrze).
2. *PHA-based inclusion complexes with cyclodextrin – preparation and degradation study* (Proiect de schimburi interacademice dintre Academia Română (ICMPP, Iași) și Academia de Științe a Poloniei (Centre of Polymer and Carbon Materials Polish Academy of Sciences, Zabrze).
3. Abordare originală în adaptarea foto/piezo actuației coexistente pe suporturi poliimidice pentru electronica flexibilă/extensibilă și senzori, project **PN-III-P1-1.1-TE-2021-1044**, contract no. TE 25/2022 (2022-2024).
4. Strategii inovatoare pentru reducerea pierderilor optice prin materiale polimerice de protecție pentru dispozitive fotovoltaice mai eficiente, project **PN-III-P1-1.1-TE-2019-1878,** contract no. TE 83/2020 (2020-2022).

## REFERENCES


Szycher M. Szycher's Handbook of Polyurethanes, Second Edition, CRC Press, Boca Raton, USA, 2013.

Arslan M., Sanyal R., Sanyal A. Cyclodextrin embedded covalently crosslinked networks: Synthesis and applications of hydrogels with nano-containers. Polymer Chemistry, 11, 615–629, 2020.

Seidi F., Jin Y., Xiao H. Polycyclodextrins: Synthesis, functionalization, and applications. Carbohydrate Polymers, 242, 116277, 2020.

Pawar S., Shende P., Trotta F. Diversity of β-cyclodextrin-based nanosponges for transformation of actives. International Journal of Pharmaceutics, 565, 333–350, 2019.

Crini G. Review: A History of Cyclodextrins. Chemical Reviews, 114(21), 10940–10975, 2014.

Topuz F., Uyar T. Electrospinning of Cyclodextrin Functional Nanofibers for Drug Delivery Applications. Pharmaceutics, 11(6), 6, 2019.

Carneiro S.B., Costa Duarte F.I., Heimfarth L., Siqueira Quintans J.D.S., Quintans-Júnior L.J., Veiga Júnior V.F.D., Neves de Lima A.A. Cyclodextrin-Drug Inclusion Complexes: In Vivo and In Vitro Approaches. International Journal of Molecular Sciences, 20, 642, 2019.

Loftsson T., Brewster M.E. Pharmaceutical Applications of Cyclodextrins: Basic Science and Product Development. Journal of Pharmacy and Pharmacology, 62, 1607–1621, 2010.

Menezes P.D.P., Andrade T.D.A., Frank L.A., de Souza E.P.B.S.S., Trindade G.D.G.G., Trindade I.A.S., Serafini M.R., Guterres S.S., Araújo A.A.d.S. Advances of Nanosystems Containing Cyclodextrins and Their Applications in Pharmaceuticals. International Journal of Pharmaceutics, 559, 312–328, 2019.

Syeda S.E.Z., Nowacka D., Khan M.S., Skwierawska A.M. Recent Advancements in Cyclodextrin-Based Adsorbents for the Removal of Hazardous Pollutants from Waters. Polymers, 14, 2341, 2022.

Liu Y., Chen Y., Gao X., Fu J., Hu L. Application of Cyclodextrin in Food Industry. Critical Reviews in Food Science and Nutrition, 62(10), 2627–2640, 2020.

Kost B., Brzezinski M., Socka M., Basko M., Biela T. Biocompatible Polymers Combined with Cyclodextrins: Fascinating Materials for Drug Delivery Applications. Molecules, 25, 3404, 2020.

Selvasembian R., Gwenzi W., Chaukura N., Mthembu S. Recent advances in the polyurethane-based adsorbents for the decontamination of hazardous wastewater pollutants. Journal of Hazardous Materials, 417, 125960, 2021.

Nagy T., Antal B., Dékány-Adamoczky A., Karger-Kocsis J., Zsuga M., Keki S. Uncatalyzed reactions of 4,4′-diphenylmethane-diisocyanate with polymer polyols as revealed by matrix-assisted laser desorption/ionization mass spectrometry. RSC Advances, 6, 47023–47032, 2016.

De Hoffmann E., Stroobant V. Mass Spectrometry - Principles and Applications. Third Edition, Chichester, West Sussex, England, 2007.

Wang L., Li L.L., Fan Y.S., Wang H. Host-guest supramolecular nanosystems for cancer diagnostics and therapeutics. Advanced Materials, 25, 3888–3898, 2013.

Hettiarachchi G., Nguyen D., Wu J., Lucas D., Ma D., Isaacs L., Briken V. Toxicology and drug delivery by cucurbit[n]uril type molecular containers. PLOS ONE, 5, 2–11, 2010.